Transition between the Okinawa Trough Backarc Extension and the Taiwan Collision: New Insights on the Southernmost Ryukyu Subduction Zone

SHU-KUN HSU[1,2], JEAN-CLAUDE SIBUET[1], SERGE MONTI[1], CHUEN-TIEN SHYU[3] and CHAR-SHINE LIU[3]

[1] *Ifremer, Centre de Brest, BP 70, 29280 Plouzané Cedex, France*
[2] *GDR 910 du CNRS, Université de Bretagne Occidentale, BP 809, 29285 Brest, France*
[3] *Institute of Oceanography, National Taiwan University, Taipei, Taiwan, ROC*

(Received 10 April 1995; accepted 18 July 1995)

Key words: Arc-arc collision, backarc extension, along-axis propagating trench, trench segmentation, Gagua ridge, Luzon arc, Taiwan, Okinawa trough.

Abstract. Located between the Okinawa trough (OT) backarc basin and the collisional zone in Taiwan, the southernmost Ryukyu subduction zone is investigated. This area, including the southwestern portions of the OT and Ryukyu island arc (RA) and located west of 123.5° E, is named the "Taiwan–Ryukyu fault zone" (TRFZ). West of 123.5° E, the OT displays NNW–SSE structural trends which are different in direction from the ENE–WSW trending pattern of the rest of the OT. Using joint analysis of bathymetric, magnetic, gravity and earthquake data, three major discontinuities, that we interpret as right-lateral strike-slip faults (Faults A, B and C), have been identified. These faults could represent major decouplings in the southern portion of the Ryukyu subduction zone: each decoupling results in a decrease of the horizontal stress on the portion of the RA located on the eastern side of the corresponding fault, which allows the extension of the eastern side of OT to proceed more freely.

We demonstrate that the 30° clockwise bending of the southwestern RA and the consecutive faulting in the TRFZ are mainly due to the collision of the Luzon arc with the former RA. After the formation of Fault C, the counterclockwise rotated portion of the ancient RA located west of the Luzon arc was more parallel to the Luzon arc. This configuration should have increased the contact surface and friction between the Luzon arc and the ancient RA, which could have reduced the northward subduction of the Luzon arc. Thus, the westward component of the compressive stress from the collision of the Luzon arc should become predominant in the collisional system resulting in the uplift of Taiwan. Presently, because the most active collision of the Luzon arc has migrated to the central Taiwan (at about 23° N; 121.2° E), the southwestern OT has resumed its extension. In addition, the later resistent subduction of the Gagua ridge could have reactivated the pre-existing faults A and B at 1 M.y. ago and present, respectively. From 9 to 4 M.y., a large portion of the Gagua ridge probably collided with the southwestern RA. Because of its large buoyancy, this portion of the ridge resisted to subduct beneath the Okinawa platelet. As a result, we suggest that a large exotic terrane, named the Gagua terrane, was emplaced on the inner side of the present Ryukyu trench. Since that period, the southwestern portion of the Ryukyu trench was segmented into two parallel branches separated by the Gagua ridge: the eastern segment propagated westward along the trench axis while the western segment of the trench retreated along the trench axis.

Marine Geophysical Researches **18:** 163–187, 1996.

1. Introduction

The Okinawa trough (OT), located landward the Ryukyu island arc (RA), is a backarc basin developed in a continental domain (Figure 1) (Lee *et al.*, 1980; Letouzey and Kimura, 1985; Sibuet *et al.*, 1987). Because the OT terminates at the western limit of the Ilan plain (northeastern Taiwan), where the Lishan fault begins (Figures 1 and 2b), the initial formation of the OT was therefore frequently considered to be associated with the collisional process in Taiwan (Letouzey and Kimura, 1985; Suppe, 1984; Teng, 1990; Angelier, 1990). In other words, previous interpretations were based on an arc-continent collision model which suggests a continuous evolution from a compressional regime to an extensional regime, such as the lateral extrusion model of Letouzey and Kimura (1985). However, the existence of NS structural discontinuities found in the Ilan plain (Hsu *et al.*, 1996) raises fundamental questions about the collision-controlled models of the OT opening. A recent arc-arc collision model, proposed by Hsu and Sibuet (1995) and Hsu *et al.* (1995), suggests that a former subduction zone extended from southwestern Taiwan to southern Japan prior to the uplift of Taiwan. In this hypothesis, Taiwan mountain building started after the closure of the oceanic domain located between the Luzon arc and the former RA. The Hsüeshan and the Backbone ranges, located on the western and eastern sides of the Lishan fault respectively, are therefore interpreted as the closure of a former backarc basin and the Tananao complex as part of the former Ryukyu arc.

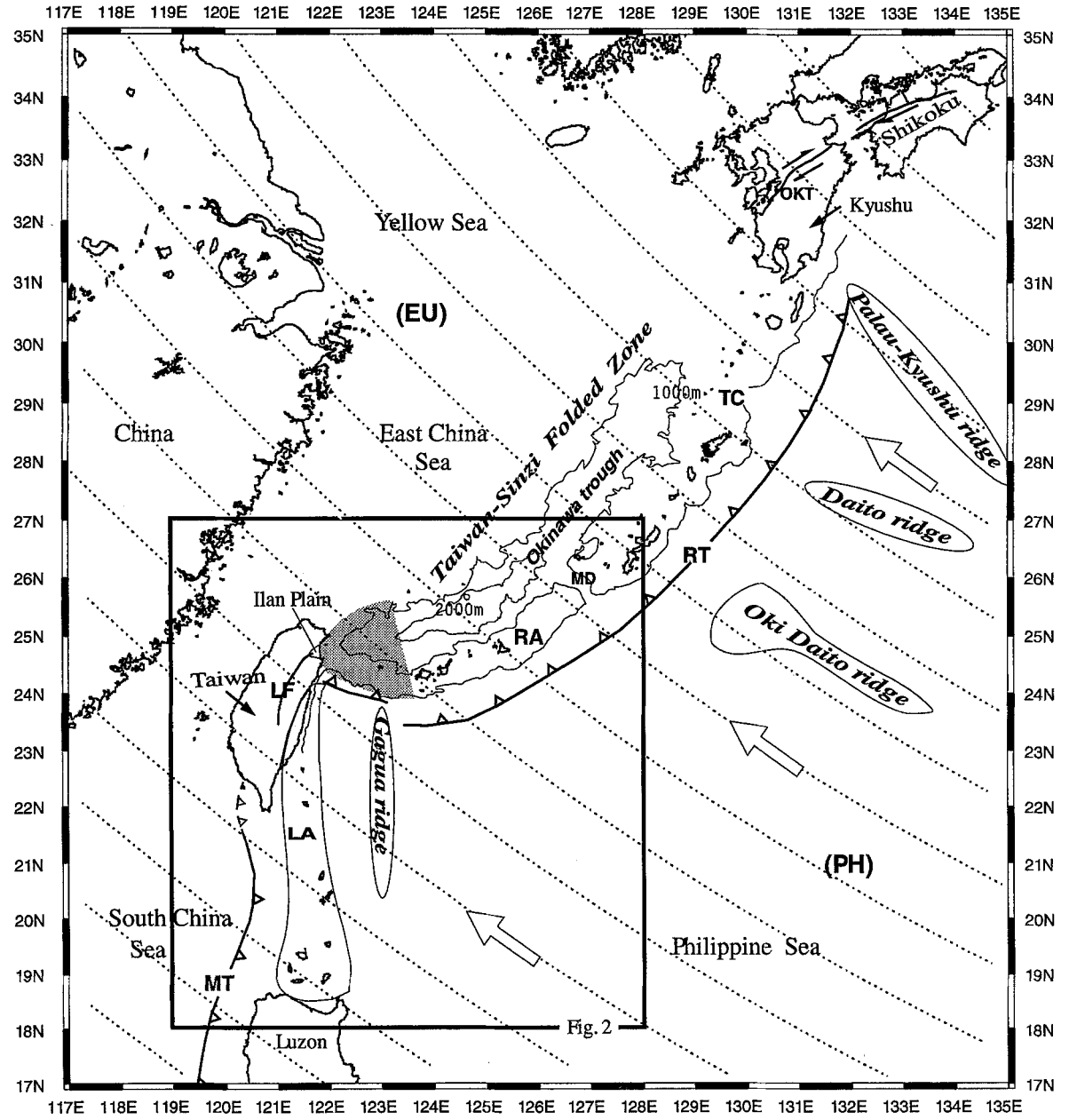

Fig. 1. Schematic context showing the intermediate zone (shaded zone) between the collision in Taiwan and the Okinawa trough (OT) backarc basin. OKT: Oita-Kumamoto tectonic line; RA: Ryukyu arc; RT: Ryukyu trench; MT: Manila trench; LF: Lishan fault; MD: Miyako depression; TC: Tokara channel; LA: Luzon arc; EU: Eurasian plate; PH: Philippine Sea plate. Dashed lines and open arrows represent the small circles and the directions of motions of PH with respect to EU, according to Seno *et al.* (1993).

The region of the present-day southernmost Ryukyu subduction zone is named the Taiwan–Ryukyu fault zone (TRFZ) (shaded zone in Figure 1). This region is located west of 123.5° E and includes the southwestern portions of the OT and Ryukyu island arc (RA). Southwest of the TRFZ, the collisional processes dominate the uplift of Taiwan, while east of this zone, the OT tensional features are not or are only weakly affected by the Luzon arc collision, as evidenced by the regular shape of the Ryukyu subduction zone. The TRFZ still exhibits tensional features within the backarc basin as attested by active extensional focal mechanism of earthquakes (Yeh *et al.*, 1991; Cheng *et al.*, 1992). However, even if this area is not directly involved

in the uplift processes in Taiwan, the abnormal curvature of the RA suggests that the Taiwan collision process has affected this area. Consequently, the TRFZ provides a natural laboratory to study the interplay between backarc extensional and collisional processes.

In this paper, we propose to compile new bathymetric and gravity maps which will be used, in addition to the already compiled magnetic map (Sibuet *et al.*, 1995), to jointly identify geologic boundaries. The interpretation of these features will help to better understand how and why the RA bends in its southwestern portion and why the OT disappears in northeastern Taiwan.

2. New Bathymetric Map

In this section, we present a new bathymetric map (Figure 2a). The digital data consist of 87 oceanic cruises extracted from the National Geophysical Data Center (NGDC) and the Institute of Oceanography of National Taiwan University data banks (Table I, Figure 3 and Plate 1 (at the back of this issue)). First of all, a cross-over technique was applied (Hsu, 1995) to automatically calculate all the cross-over errors (XOEs) (Figure 4). From the XOE information we define

$$W_i = N / \sum_{j=1}^{N} (\mathrm{XOE}_{i,j})^2$$

as the relative weighting function which represents the data quality of each cruise (Table I). W_i is the weight for the ith cruise, $\mathrm{XOE}_{i,j}$ is the jth XOE for the ith cruise, while N represents the total number of cross-over points (XOPs) for the ith cruise. To enhance the confidence of depth estimation and to avoid pseudo-features in the contour map generated from large XOEs along ship tracks, all the XOEs at the XOPs were eliminated, and a new value was assigned at each XOP, according to the relative weights of the two intersecting cruises. Between consecutive XOPs, the rest of the data was proportionally adjusted according to the newly computed values at the two XOPs (Hsu, 1995). The root-mean-square error (rms) for all the XOEs is 119.3 meters (Figure 4b). Cruises characterized by average XOE values larger than 200 meters, an arbitrary defined truncated value, were removed. Remaining data were contoured by using the method of continuous curvature splines in tension (Smith and Wessel, 1990). However, because bathymetric data are not homogeneously distributed, the area located east of 123° E and south of 24° N was drawn by hand, taking into account the general trends given by the satellite derived marine gravity map (Sandwell *et al.*, 1994). Except that, all the iso-contours were drawn automatically without human judgement. In addition, a Seabeam map of the area located near the southwestern Ryukyu trench and Gagua ridge intersection (22°20′ N to 24°20′ N and 122°50′ E to 126°20′ E, Matsumoto *et al.*, 1993) was added. On land, the Digital Elevation Model (DEM) of Taiwan (Deffontaines *et al.*, 1994; Lee, 1994) was added into the digital dataset. For compatibility with shipboard bathymetric data, DEM data were converted into the same geographic coordinate system. The spatial resolution of the DEM data is 500 m × 500 m in the horizontal plane and about 75 m in elevation (Deffontaines *et al.*, 1994). This resolution is roughly similar to the one of the bathymetric map. A 3–D topographic model has also been produced (Figure 2b).

With respect to previously published bathymetric maps (e.g. Sibuet *et al.*, 1987), the present bathymetric map is systematically more reliable because XOEs are zero. However, for local studies (e.g. the morphology of a canyon) detailed surveys are needed. The new major features which appear on the bathymetric and topographic maps (Figures 2a and 2b) are:

1. West of 123.5° E, the OT gradually narrows and ends formally into the Ilan plain (Figure 2b). However, the backarc basin is prolonged by the deep valley corresponding to the Lishan fault. In the Hsu and Sibuet (1995) and Hsu *et al.* (1995) hypothesis, the suture zone along the Lishan fault corresponds to the closure of an uplifted former backarc basin.
2. The Gagua ridge is a pronounced linear feature trending N 004° near the 123° E meridian. It is composed of a succession of seamounts and elongated ridges.
3. The Nanao basin extends from Taiwan to 125° E. A major change in the direction of this basin appears at 123.6° E longitude. This change of direction is related to a N135° bathymetric trend cutting across the Nanao basin and extending to the RA.
4. The region located between 125.7° E and 127.7° E is a positive topographic forearc feature of the RA. It is in the eastern prolongation of the Nanao basin and is also characterized by a poor magnetic anomaly, a strong gravity anomaly and low seismicity.
5. Several pronounced bathymetric depressions trending NNE–SSW at 21° N; 122° E and NE–SW at 20° N; 122° E, separate the Luzon arc into several segments. These depressions have been interpreted as strike-slip faults (Karig, 1973) or thrust faults (Lewis and Hayes, 1989), implying that the Luzon arc is not a rigid feature. As the Luzon arc progressively changes of direction from N 345° at 20°–22° N to N 020° east of Taiwan, we suggest that the EW

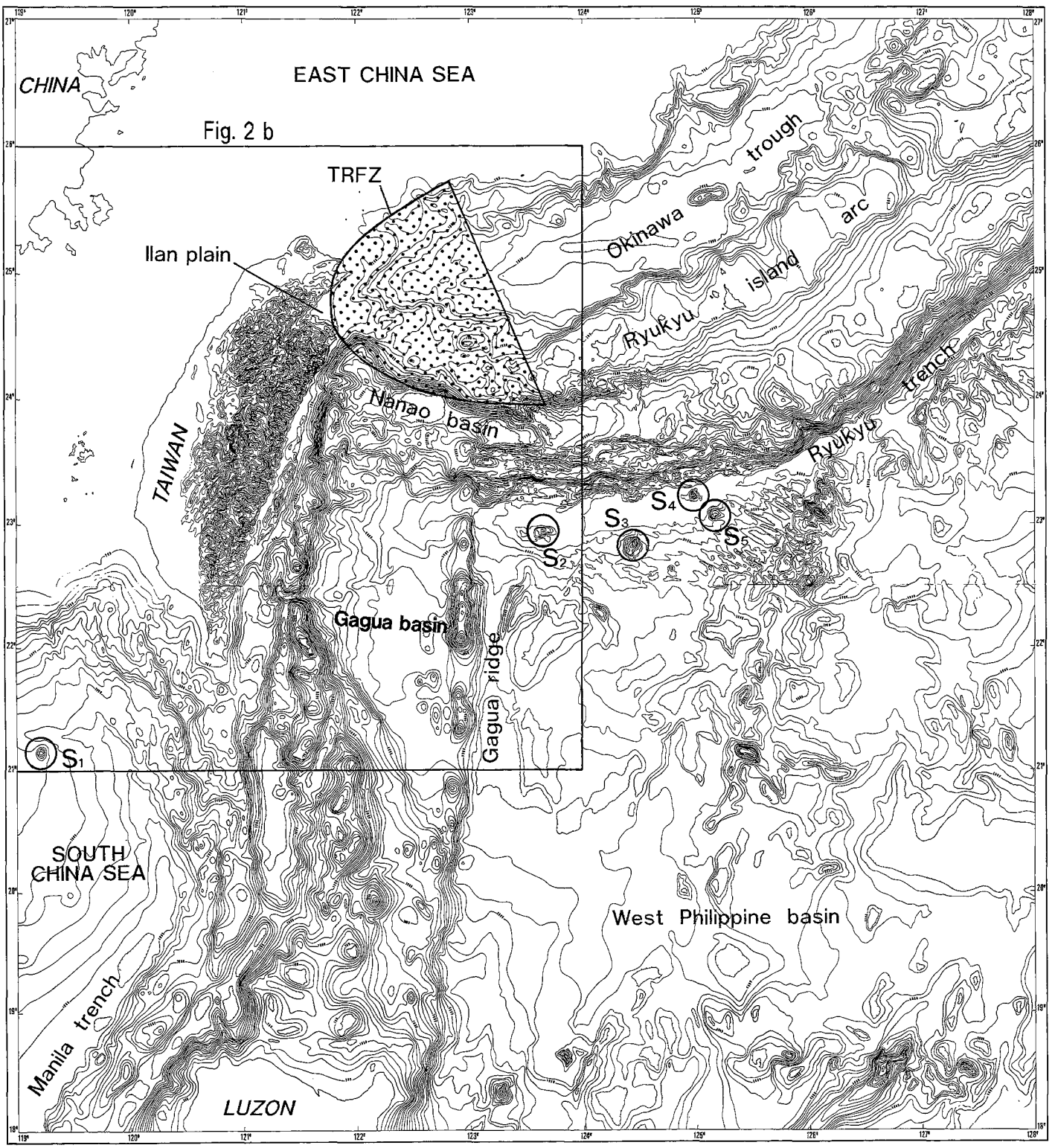

Fig. 2a. New bathymetric map around Taiwan. Mercator projection. Contour interval 200 m. Data coverage is shown in Fig. 3. See black and white foldout at the back of this issue (Plate 1). TRFZ: Taiwan-Ryukyu fault zone.

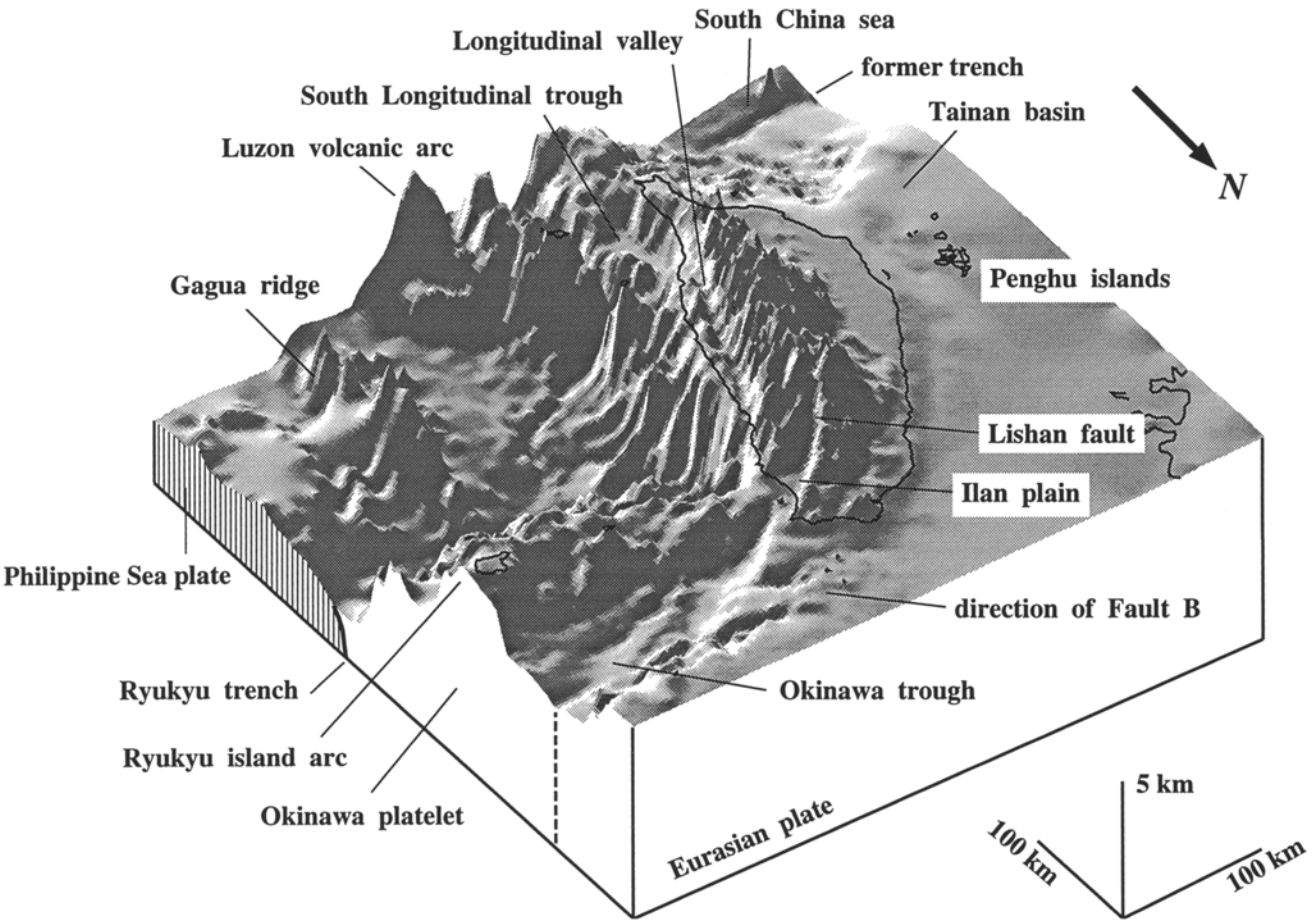

Fig. 2b. 3–D topographic relief of the area located between 21° N; 26° N and 119° E; 124° E. Note the gradual narrowing from the southwestern Okinawa trough to the Lishan fault.

depression located near 22.3° N; 121.5° E (between the islands of Lutao and Lanhsu) corresponds to a major discontinuity of the Luzon arc linked to a major change in stress conditions. Moreover, this depression is prolonged in the Gagua basin by a N 070° feature, along which several earthquakes of magnitude larger than 6 indicate a dextral strike-slip motion. This motion is also confirmed by the marine gravity anomalies (Sandwell et al., 1995), which shows a right-lateral offset of the trends between the Lutao and Lanhsu islands. In addition, the bathymetric map shows that the eastern side of the Luzon arc seems to be limited by a linear feature trending NW–SE, roughly along the 4000-m isobath (21.5° N; 122° E).

6. The width of the Luzon arc progressively decreases in the northward direction to almost zero at 24° N. Taking into account the geodetic information of Yu *et al.* (1995), it implies that the Luzon arc could have begun to subduct beneath Taiwan at least north of 23.5° N.
7. In eastern Taiwan, the Longitudinal valley is considered as the suture zone between the former Ryukyu arc and the Luzon arc (Hsu et Sibuet, 1995; Hsu *et al.*, 1995). This suture zone is probably connected to the Nanao basin, as shown by the continuity of the topographic depressions from the northern end of the Longitudinal valley to the western end of the Nanao basin.
8. NW–SE directions which appear in the Philippine Sea close to the Ryukyu trench (between 125° E and 126° E) on the Japanese swath bathymetric survey (Matsumoto *et al.*, 1993) correspond to the oceanic rift fabric formed at the time of magnetic anomaly 20 (Hilde and Lee, 1984).
9. Several new seamounts (S1 to S5) have been identified in the oceanic domain, close to the Ryukyu trench.

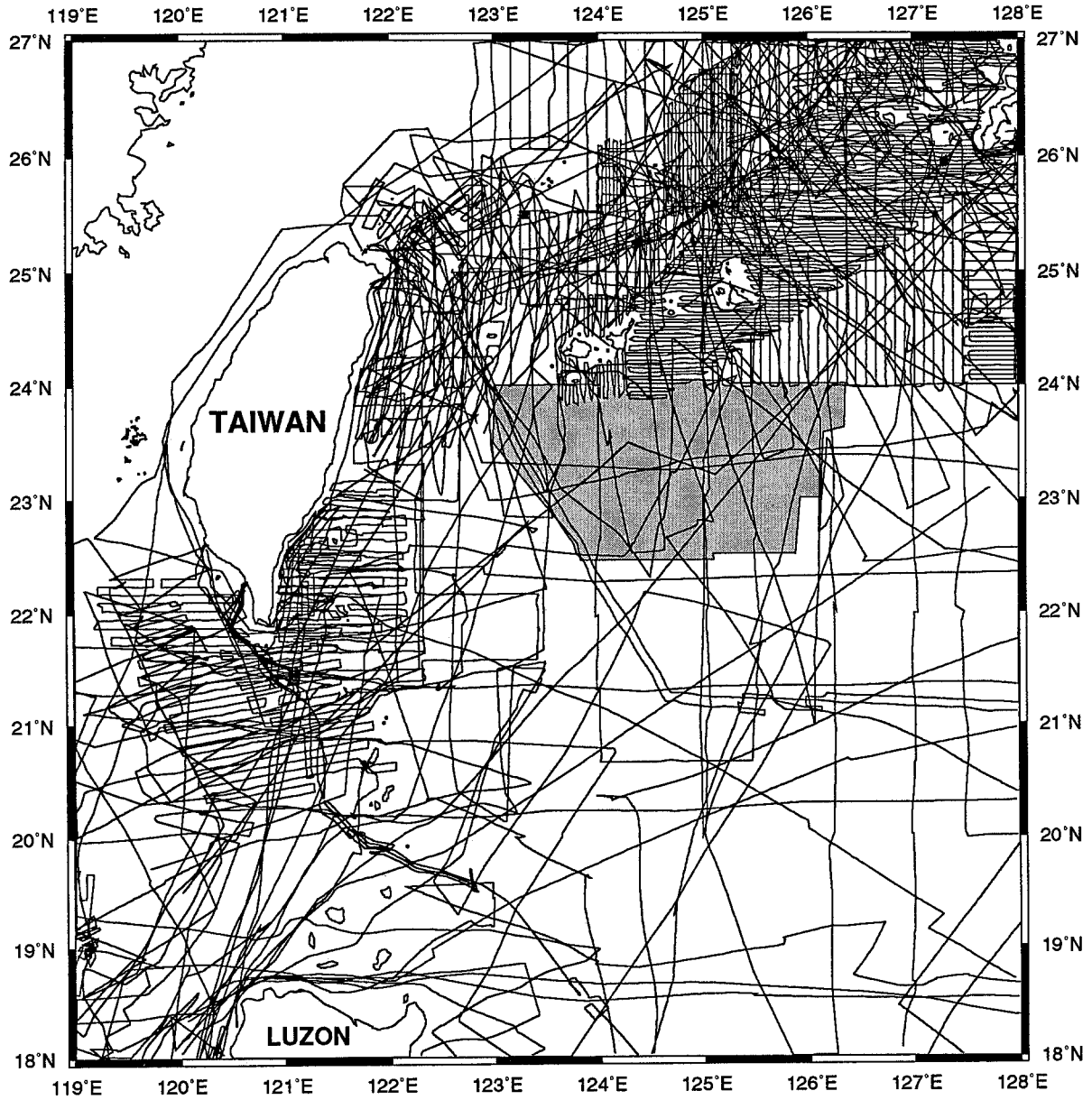

Fig. 3. Bathymetric ships' tracks used in this study. The identification and data quality of each cruise are shown in Table I. The shaded area corresponds to the Seabeam survey of Matsumoto *et al.* (1993) added in Fig. 2a.

10. West of 120° E, the continental margin is supposed to be a former subduction zone (Hsu and Sibuet, 1995 and Hsu *et al.*, 1995). The location of the paleo-trench would correspond to the EW depression parallel to 21.3° N. This segment of paleo-trench could be connected to the Longitudinal valley through the southward offshore extension of the Longitudinal valley (i.e. the South Longitudinal trough) (Figure 2b).

3. New Gravity Anomaly Map

To determine the geological boundaries, new free-air and Bouguer gravity anomaly maps have been produced. The shipboard gravity data have been extracted from the NGDC data base. Gravity data have been acquired during 53 different cruises (Figure 5) and re-corrected by the IAG system 1967. After correction, the rms of the total XOEs is 14.4 mGal (Figure 6). Then, all the XOEs have been eliminated

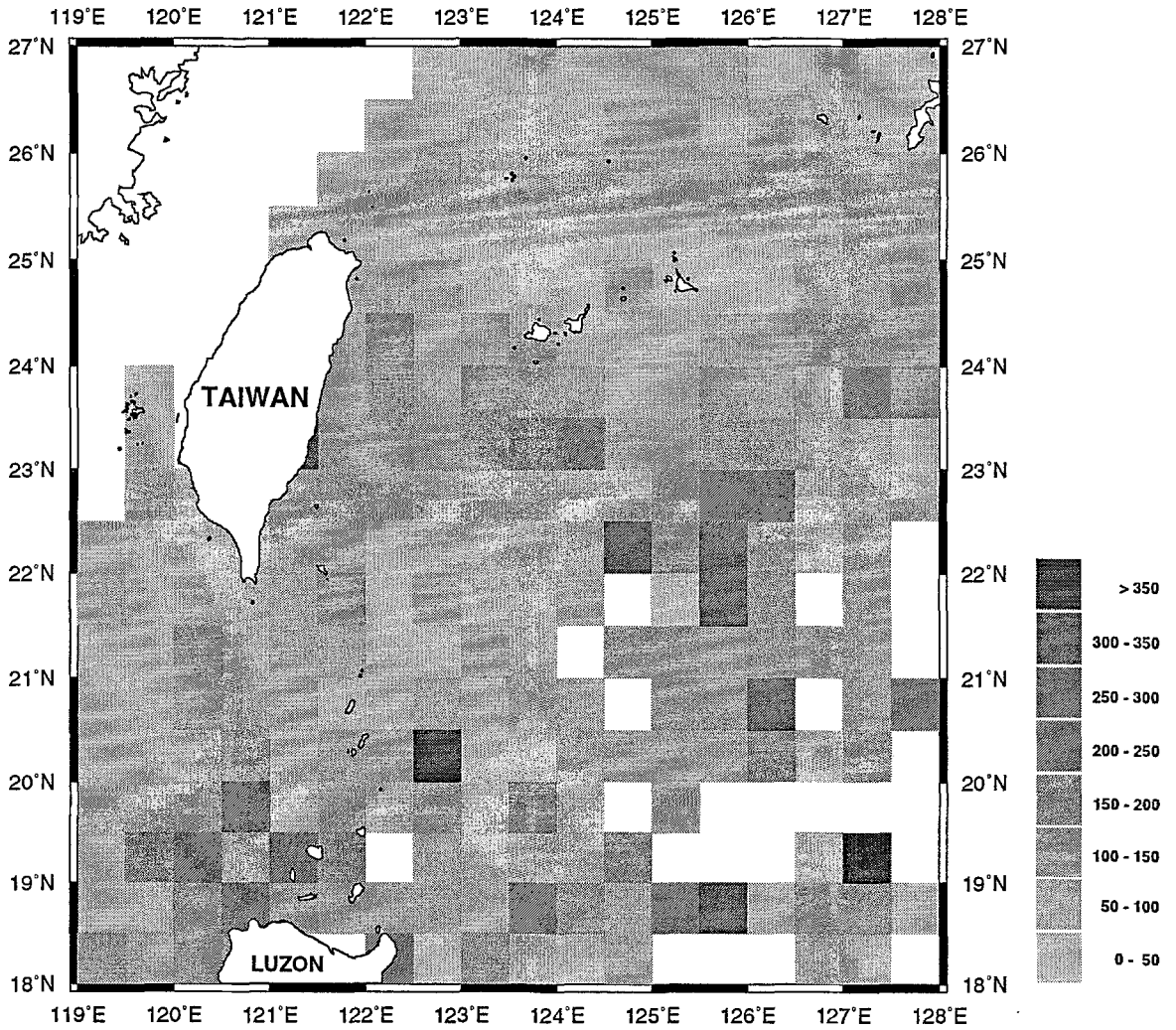

Fig. 4a. Average XOE of bathymetric cruise data for each 0.5 x 0.5 square degree. Unit in meters.

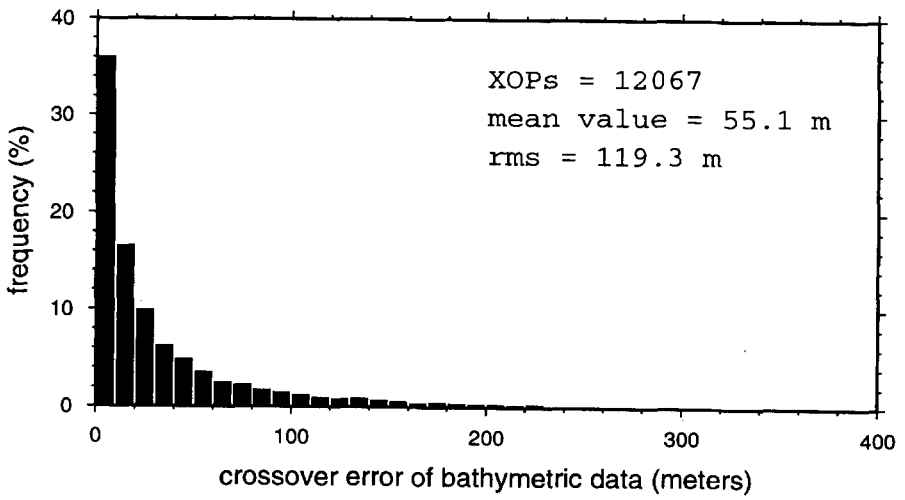

Fig. 4b. Histogram of bathymetric XOEs for cruise data shown in Table 1.

TABLE I
Crossover analysis of bathymetric cruises used in this study

Cruise	Start date	XOP (internal)	XOP (external)	Average XOE (meters)	Relative weight
IRI325	July 26, 1992	132	169	36.5	0.817
84001311	May 14, 1984	0	80	57.8	0.715
84003211	Sept. 21, 1984	61	1163	38.0	1.413
84004211	Oct. 18, 1984	66	439	56.0	0.776
84004711	Nov. 13, 1984	0	10	89.1	0.652
A2015L04	June 27, 1965	3	296	99.9	0.390
ANDAC21B	(unknown)	0	193	32.8	1.823
ANTPO4MV	Aug. 28, 1970	3	69	108.2	0.241
C1217	May 28, 1969	1	124	97.2	0.444
C1404	May 9, 1971	0	314	47.1	1.128
C1710	Aug. 15, 1974	3	236	60.8	0.620
C1711	Sept. 16, 1974	0	114	52.8	1.225
C2006	Jan. 26, 1976	0	142	80.3	0.397
C2007	Dec. 3, 1976	16	402	32.9	2.145
C2008	Dec. 23, 1976	0	69	64.6	0.855
C2009	Jan. 5, 1977	3	91	84.8	0.559
DME10	June 27, 1973	0	25	97.0	0.289
DME24	Jan. 22, 1980	0	107	47.9	1.186
DSDP31GC	June 15, 1973	1	20	73.2	1.096
GH7501	Jan. 19, 1975	46	978	68.4	0.524
GH7505	July 16, 1975	7	186	50.8	1.030
HS7501	Apr. 10, 1975	125	171	10.9	3.533
HST602	Apr. 12, 1976	231	1463	49.7	1.094
HS7603	June 4, 1976	137	592	35.9	2.861
HS8202	Apr. 10, 1982	160	758	47.5	0.824
HT8402	June 22, 1984	39	589	34.4	1.944
HT8403	Oct. 14, 1984	65	675	33.8	1.875
HT8502	Oct. 5, 1985	311	1862	43.6	1.128
HT8612	Dec. 5, 1986	12	113	54.0	1.457
HT8701	Oct. 9, 1987	11	63	86.6	0.633
HT861016	Oct. 16, 1986	0	5	53.2	1.513
HT861102	Nov. 2, 1986	0	33	36.9	3.016
HU939013	June 14, 1969	0	122	88.3	0.324
HUNT01HT	Oct. 6, 1969	1	160	96.1	0.325
INDP03WT	May 25, 1976	2	105	108.2	0.312
INDP05WT	July 8, 1976	23	173	29.9	2.297
INDP06WT	July 31, 1976	3	160	62.8	0.863
KH7104	Jan. 21, 1971	0	106	81.2	0.384
KH7201	May 11, 1972	0	63	161.8	0.167
KH7202	Jan, 25, 1972	2	351	80.7	0.554
KH7403	July 19, 1974	1	164	192.8	0.088
KH7501	Jan. 10, 1975	0	171	69.3	1.021
KH7502	Feb. 15, 1975	3	53	57.0	1.289
KH7505	Sept. 13, 1975	0	22	38.0	2.637
KH7605	Dec. 22, 1976	0	209	88.8	0.367
KH7802	Apr. 20, 1978	2	23	27.5	4.341
KH79	Jan. 27, 1979	2	351	59.5	0.641
MW8803	Mar. 12, 1988	352	399	29.4	2.247
MW9006	May 4, 1990	223	900	50.4	1.009
CDP124EJ	Jan. 9, 1989	30	89	138.4	0.132
CRI183	Oct. 11, 1988	6	157	103.6	0.173
ORI200	Mar. 15, 1989	0	101	117.2	0.290
ORI211	May 25, 1989	9	180	112.0	0.325
ORI222	Aug. 17, 1989	0	58	117.3	0.384
ORI232	Nov. 4, 1989	1	25	160.5	0.182
ORI279	Apr. 25, 1991	31	148	83.6	0.510
ORI291	Aug. 5, 1991	27	305	55.8	0.803

TABLE I (Continued)

Cruise	Start date	XOP (internal)	XOP (external)	Average XOE (meters)	Relative weight
ORI298	Oct. 12, 1991	9	284	72.0	0.377
ORI326	Aug. 1, 1992	43	188	29.2	1.859
ORI336	Nov. 22, 1992	87	86	39.3	0.558
POL6202	Apr. 4, 1962	0	14	62.4	1.498
POL7202	Mar. 7, 1972	18	443	94.3	0.263
ST939011	Feb. 13, 1969	2	264	69.1	0.505
ST	------, 1969	0	71	108.5	0.380
UM68	Oct. 16, 1968	0	115	104.4	0.301
UM69	Oct. 26, 1969	0	47	111.7	0.284
V2107	June 15, 1965	5	261	132.0	0.201
V2108	July 8, 1965	11	178	95.7	0.454
V2110	Aug. 8, 1965	0	42	166.9	0.133
V2405	Apr. 25, 1967	0	41	170.1	0.094
V2406	May 31, 1967	5	73	80.4	0.445
V2817	Aug. 13, 1971	9	468	58.2	0.802
V3310	Aug. 27, 1976	11	501	44.8	0.677
V3613	June 28, 1980	6	157	103.6	0.173

by linear adjustment to avoid linear pseudo-structures as previously mentioned. The free-air gravity anomaly map (Figure 7a) has been obtained by contouring the adjusted data with the GMT-free software (Wessel and Smith, 1991). To obtain the Bouguer anomaly (Figure 7b), the bathymetric and free-air gravity anomaly datasets were gridded in a similar manner ($5' \times 5'$) and the water effect of each $5' \times 5'$ rectangular prism was replaced by a sedimentary prism of density 1.67 g/cm^3. Because of the limited extent of the bathymetric map, the edge effect is not corrected on the Bouguer anomaly map. However, this effect is limited to the borders of the map.

4. Identification of Three Major Discontinuities

To outline geological boundaries such as faults or contacts, a second-order enhanced analytical signal technique has been used (Hsu *et al.*, 1996). This method helps to locate the geological boundaries by tracing the maximum amplitudes of second-order enhanced analytical signal which is composed of the curvature values of the two horizontal and the vertical derivatives of the potential field anomalies. The relationship between each maximum amplitude and the depth from the measured surface to the top surface of the boundary corresponds to a peak of a bell-shaped function and is expressed as:

$$|A_2|_{\max} = \left| \sqrt{\left(\frac{\partial^2 G_x}{\partial z^2}\right)^2 + \left(\frac{\partial^2 G_y}{\partial z^2}\right)^2 + \left(\frac{\partial^2 G_z}{\partial z^2}\right)^2} \right|_{\max} = \frac{|2\alpha|}{d^3}$$

where G is the gravity (or the magnetic anomaly);

$$G_x = \frac{\partial G}{\partial x}; \quad G_y = \frac{\partial G}{\partial y}; \quad G_z = \frac{\partial G}{\partial z};$$

d is the distance to the top surface of the causative source;

α is a coefficient of ambient parameters such as the intensity, inclination and declination of magnetization or the density contrast of the gravity source.

For a simple estimation of the depth d, the amplitude ratio method (Hsu *et al.*, 1996) is used:

$$d \cong \sqrt{2} \times \sqrt{\frac{|A_0|}{|A_2|_{\max}}}$$

where

$$|A_0| = |\sqrt{(G_x)^2 + (G_y)^2 + (G_z)^2}|.$$

The major advantages of this technique are:

1. The interference effect between close anomalies is reduced.
2. The determined locations of maximum amplitudes are independent of ambient parameters (such as inclination and declination of magnetization).

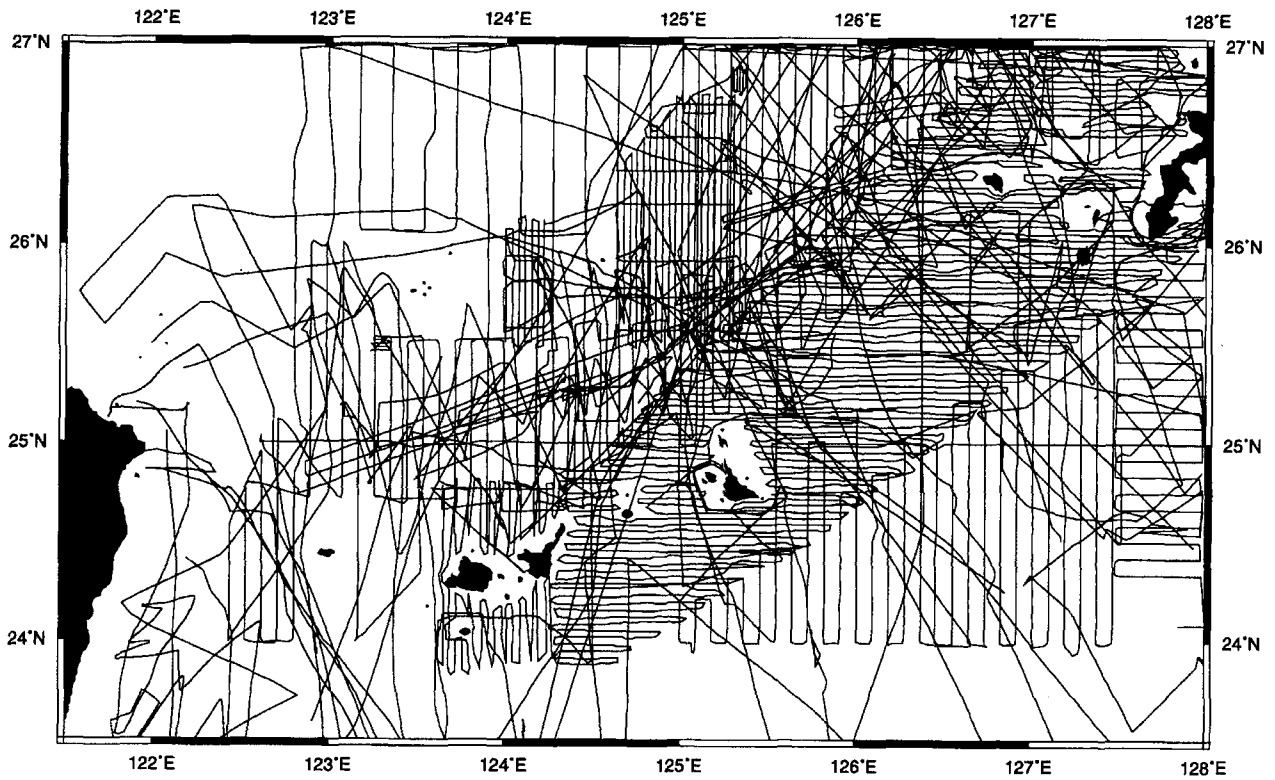

Fig. 5. Gravity ships' tracks used in this study.

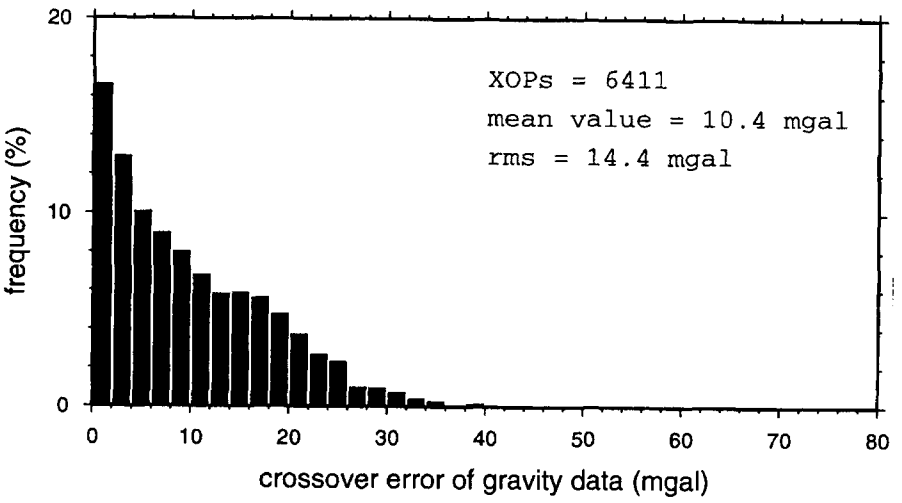

Fig. 6. Histogram of XOEs of gravity anomalies compiled in this study.

3. The determination of maximum amplitudes can be automatically achieved by examining every 9–point grid-cell (Blakely and Simpson, 1986).

However, for real data, the topographic effect and the high frequency error render this method less powerful. For that reason, we have used both the gravity anomalies presented here and the magnetic anomalies (Figure 8) compiled by Sibuet *et al.* (1995) to determine the geological boundaries. In addition, to avoid contour artefacts due to an insufficient density of shipboard

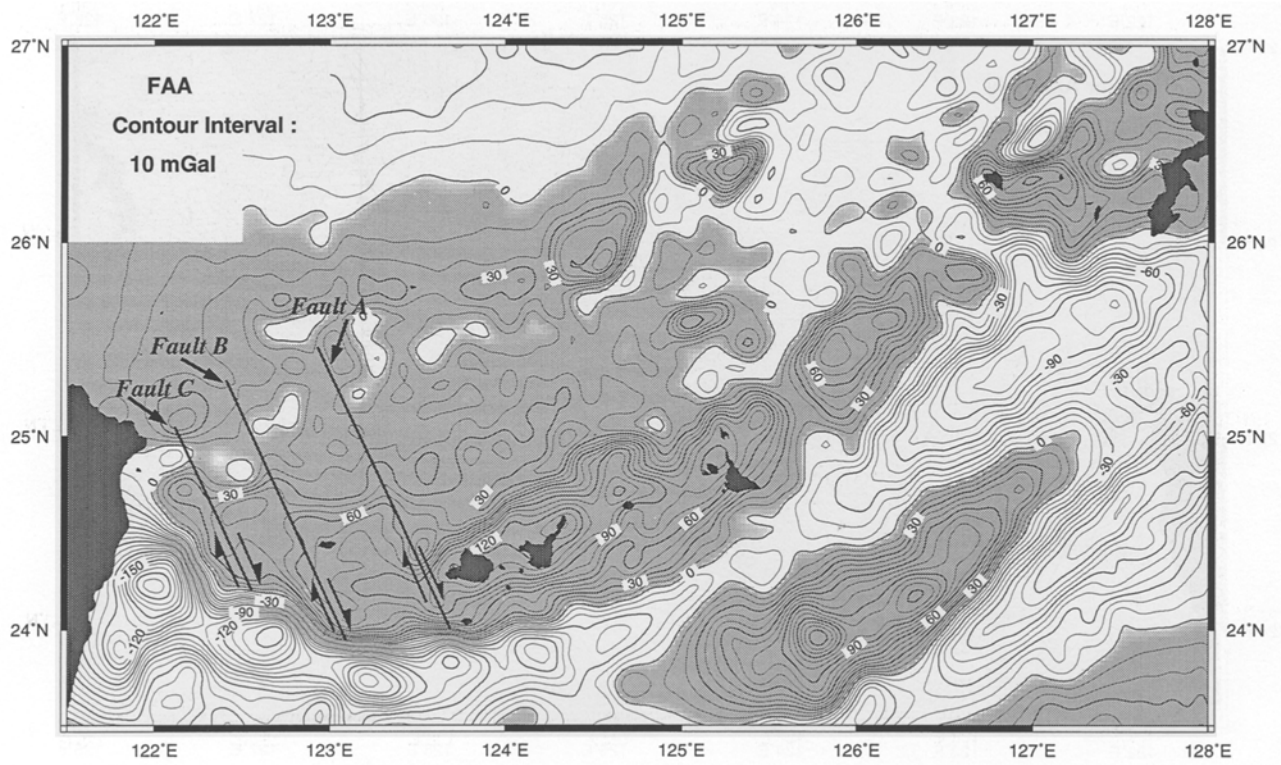

Fig. 7a. Free-air gravity anomaly map of the southwestern OT. Positive values are shaded. Note that the step-like form of the steepest slope from 24.3° N; 122° E to 24° N; 123.5° E also reveals the locations of the right-lateral faults based on the maximum horizontal-gradient method (Cordell and Grauch, 1985).

data, a low-pass gaussian filter of 15 km has been applied to the gridded data sets before applying the enhanced analytic signal method.

The locations and depths to the top surfaces of geological boundaries have been identified by using both gravity and magnetic anomalies (Figures 9 and 10). For better understanding, the continuation of boundaries has been drawn by hand. A careful examination of the identified boundaries with the bathymetric map shows that the topographic effect is dominant, especially on the OT margins. Among the detected boundaries, three major structural boundaries (discontinuities) trending roughly NW–SE appear in the southwestern OT (Faults A, B and C in Figure 7a to Figure 12). For comparison these discontinuities are plotted at the same location on each figure. The enhanced analytic signals associated with the three discontinuities are weak but their existence is confirmed by the abrupt truncation of several roughly NE–SW trending boundaries. This phenomenon implies that either the contrast of physical properties on each side of these discontinuities is weak, or their throw is small. We interpret these three discontinuities as faults because they correspond to bathymetric offsets or changes in the direction on the northern RA margin (Figure 11), which suggests a dextral strike-slip motion along these faults. In addition, the northwestern ends of the three faults are connected with canyons (e.g. in regions C1 and C2 of Figure 11) which are generally consistent with the structural trends. These faults are likely to extend northwestward on the continental shelf up to about 26° N, taking into account the seismic interpretations of Huang *et al.*, (1992) and Chen and Watkins (1994) on the continental shelf of the northern Taiwan. Moreover, as shown by the epicentral distribution of the NEIC's (National Earthquake Information Center) earthquake data for magnitude greater than 4 from 1965 to 1992, the density of earthquakes varies from one side to the other side of each fault (Figures 12a and 12b). From the distribution of sedimentary patterns and focal mechanisms of earthquakes, several authors (Wageman *et al.*, 1970; Karig, 1973; Yen, 1975; Wu, 1970 and

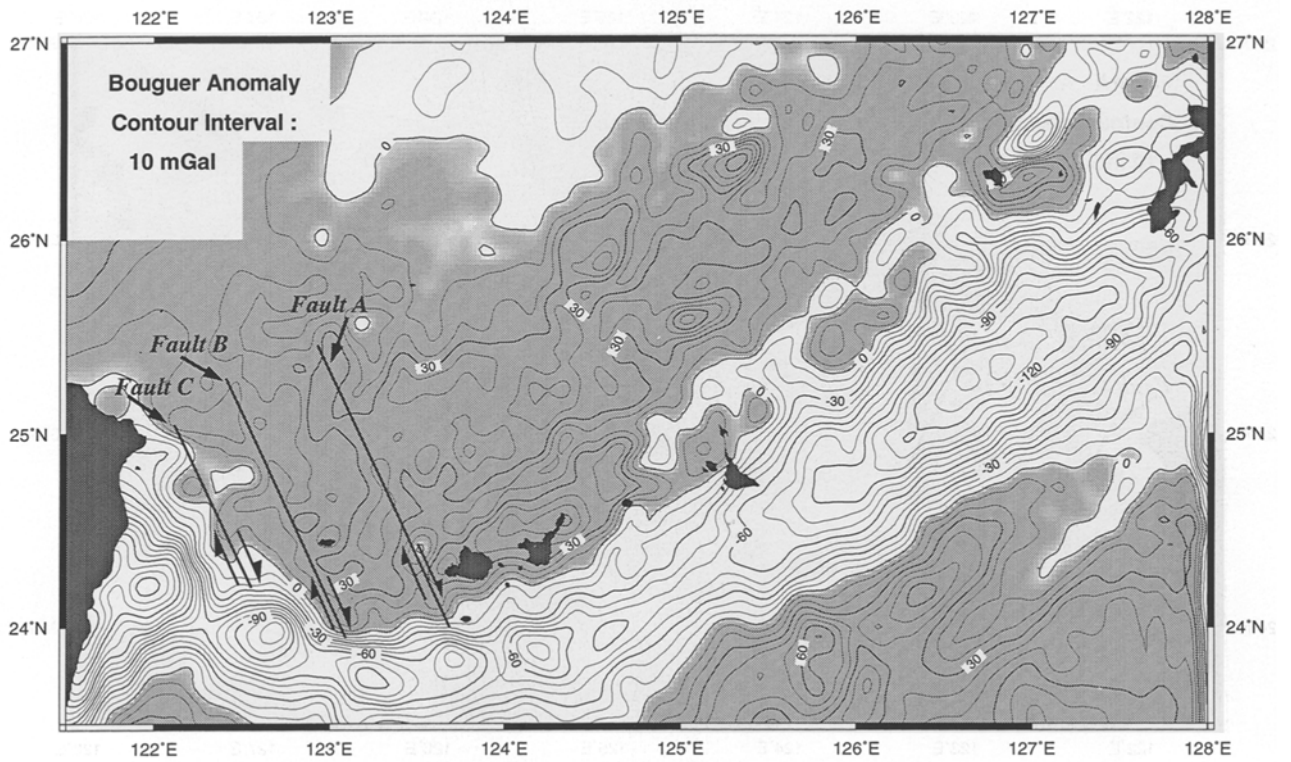

Fig. 7b. Bouguer gravity anomaly map of the southwestern OT. Each 5′ × 5′ rectangular prism of water was replaced by a sedimentary prism of density 1.67 g/cm^3.

1978; Lallemand *et al.*, 1995) have also suggested a dextral strike-slip tectonic regime in the region around the southernmost RA.

The discovery of these right-lateral strike-slip faults provides a very important constraint for the tectonic evolution of the southernmost Ryukyu subduction zone because: (1) They are continuous features that extend from the arc to the backarc region and the continental shelf. As evidenced by the depths of the earthquakes, the faulting could reach 30 km deep in the crust (Figure 12b); (2) Though no transform faults or fracture zones have been observed in the whole Okinawa trough (Sibuet *et al.*, 1987), the NNW–SSE orientation of Faults A, B and C might suggest that these faults are reactivated backarc basin fracture zones because they are quite parallel to the theoretical direction of the OT fracture zones (Sibuet *et al.*, 1995). Nevertheless, because they are continuous features and could be produced by an external force (indentation process) acting on the RA (see later), it is more probable that they represent dextral strike-slip faults.

5. Indentation Tectonics of the Southwestern Ryukyu Subduction Zone

Because of data density and in order to reduce the topographic effect, a 20–60 km gaussian band-pass filter was applied to the gravity and magnetic maps. Two major provinces appear in the southern OT (Figures 13 and 14). In the eastern province (east of 123.5° E), the ENE–WSW structural trends are roughly parallel to the en-échelon extensional depressions located in the central trough. By contrast, features of the western province (west of 123.5° E) are mainly NNW–SSE oriented. These latter trends, roughly parallel to the identified Faults A, B and C, and the development of canyons help to define a distinct portion of arc and backarc region named the Taiwan-Ryukyu fault zone (TRFZ) (Figure 2a).

5.1. Bending of the southwestern Ryukyu arc

The morphology (Figure 11) shows that: (1) the two segments of bathymetric slopes located west of Faults

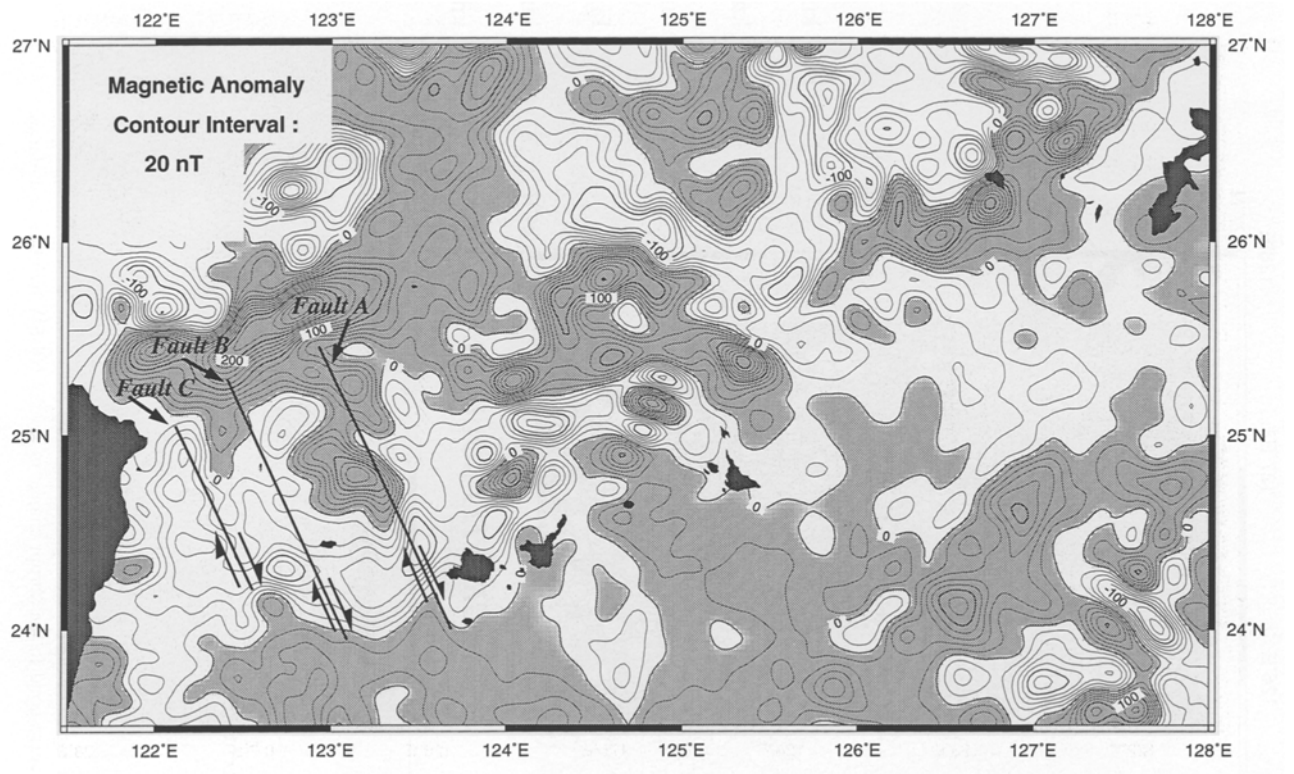

Fig. 8. Magnetic anomaly map of the southwestern OT (after Sibuet *et al.*, 1995). Positive values are shaded. Faults A, B and C are shown.

A and B (segments S1 and S2) are roughly parallel and EW oriented; (2) the segment S3, located in the non-deformed area of the Okinawa trough, is oriented N 60°. If we assume that the northern margin of the RA was formerly oriented N 60°, then the western portion of the south RA was rotated clockwise of about 30° around a pole of rotation located east of Fault A, possibly near 24° N; 123.6° E (point P in upper diagram of Figure 11). We suggest that this rotation was mainly due to the collision of the Luzon arc with the RA and mostly occurred before the initial uplift of Taiwan. The angle of rotation is, however, smaller than the total bending angle (about 50°) between the strike of the undeformed RA (parallel to segment S3) and the mean strike of the southernmost RA (west of 123.5° E). This means that part of the bending would have been accommodated by the dextral strike-slip motions along the Faults A, B and C.

Marine normal faults, generally N–S oriented, around the Miyako island (Figure 11) suggest an extensional regime east of 123.5° E, while around the Yonaguni island (at about 122.9° E, 24.4° N) the tectonic features are roughly EW oriented and the principal stress is roughly oriented NW–SE on this island (Kuramoto and Konishi, 1989). These observations suggest that, west of 123.5° E, the bent RA is still in a compressional regime.

Numerous earthquakes with compressional focal mechanisms (Cheng *et al.*, 1992) occurs within the bent RA, south of segments S1 and S2 (Figures 12a and 12b). In contrast, north of segments S1 and S2, numerous earthquakes with extensional focal mechanism occur in the OT. The large density of earthquakes, with extensional and compressional mechanisms, is geographically restricted west of 123.5° E and is significantly different from the earthquake density of the rest of the Ryukyu subduction zone. The abnormal amount of extensional earthquakes in the southwestern OT could be due to different factors such as a pressure release due to faulting or a decrease of temperature. The latter possibility is suggested by weak heat flow values (generally less than 1 HFU) recorded in the southwestern OT (Lu *et al.*, 1981) and the presence of a relatively low gravity anomaly in this area (Figures 7a and 7b).

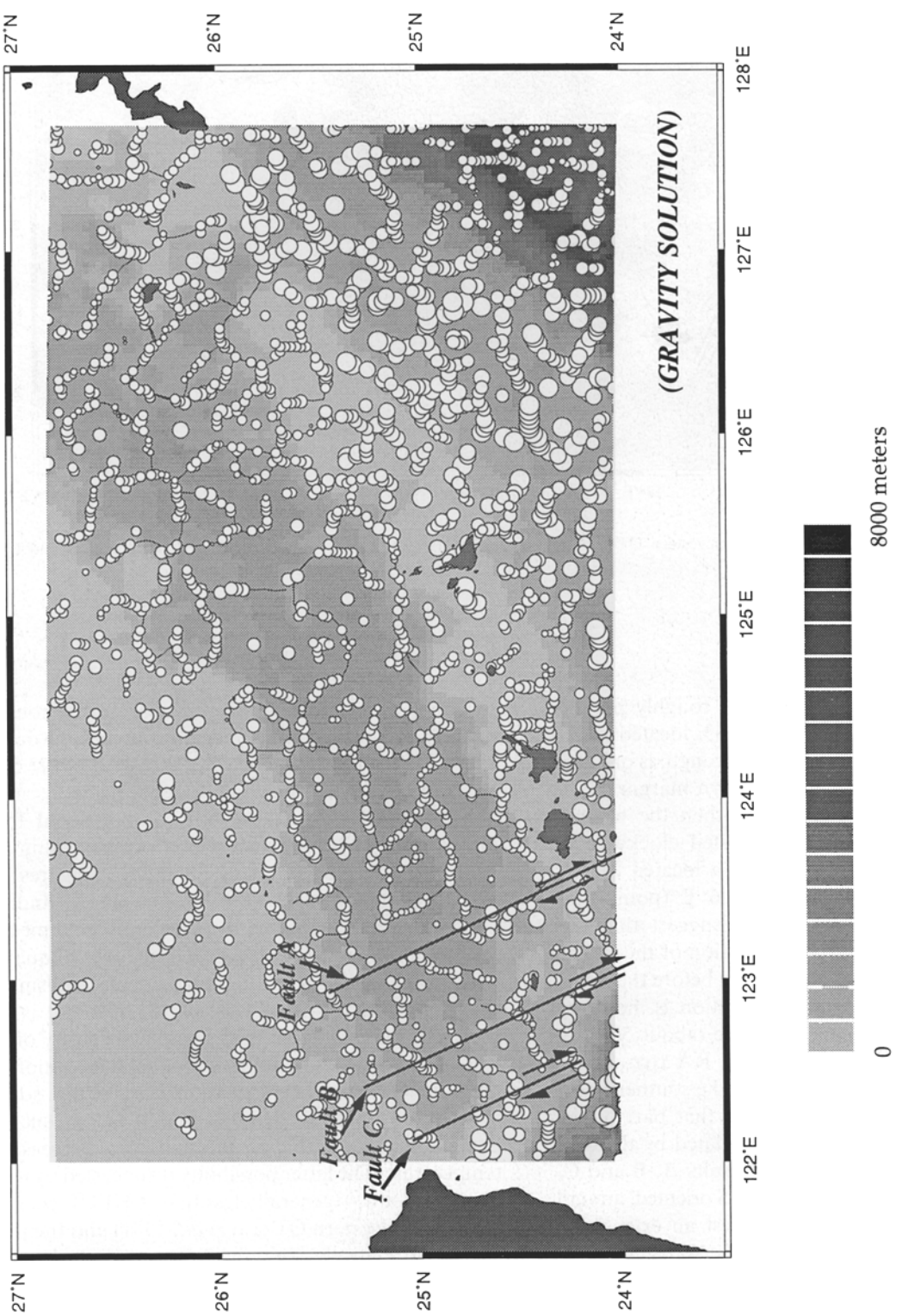

Fig. 9. Geological boundaries of the southwestern OT detected by second-order enhanced analytic signal of the Bouguer gravity anomaly (Hsu *et al.*, 1996). The shaded bathymetry is superposed. Faults A, B and C are shown. Note that locations of Faults A, B and C correspond to the abrupt change of several NE-SW trending boundaries.

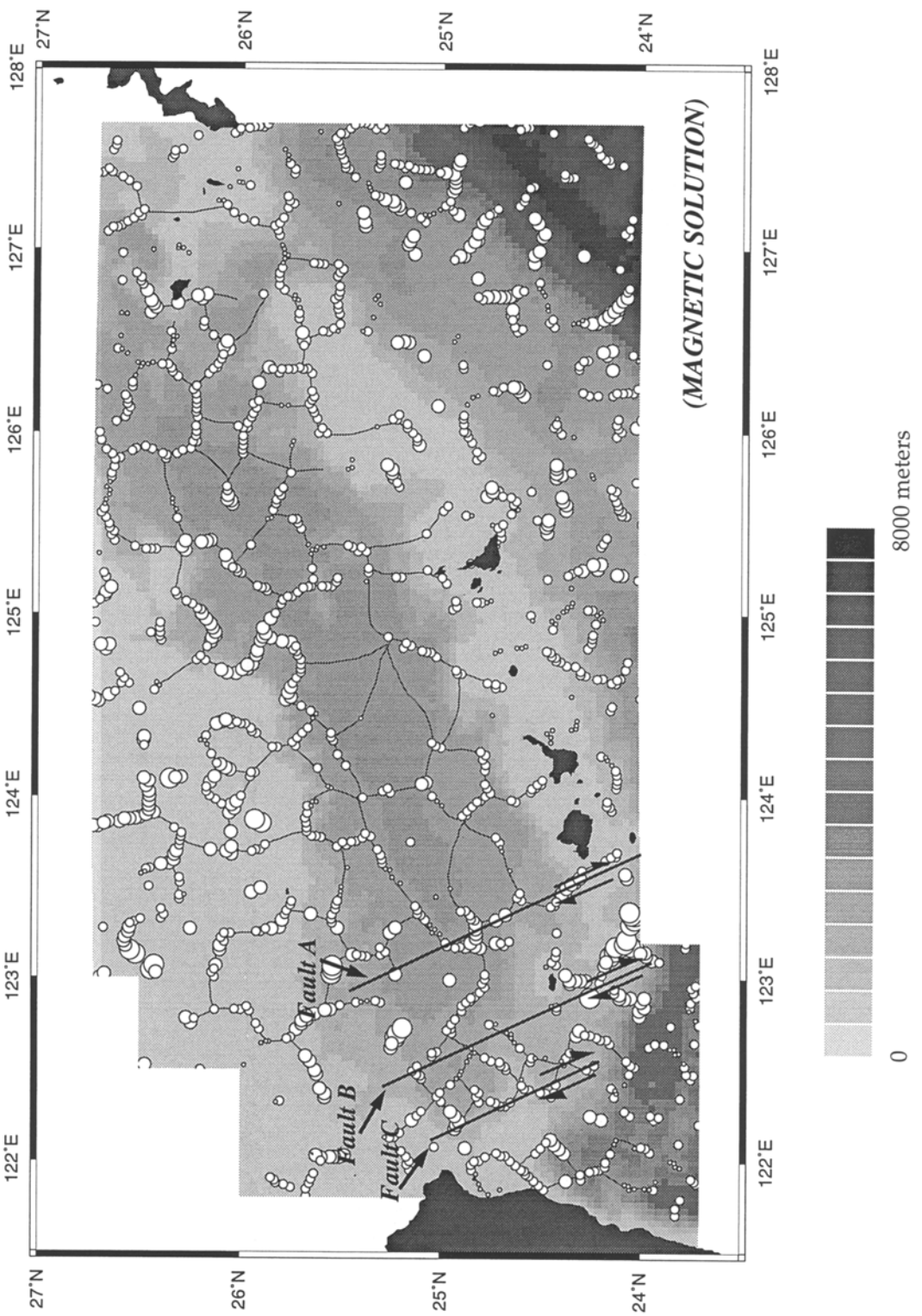

Fig. 10. Geological boundaries of the southwestern OT detected by second-order enhanced analytic signal of the magnetic anomaly (Hsu *et al.*, 1996). The shaded bathymetry is superposed. Faults A, B and C are shown. Note that locations of Faults A, B and C correspond to the abrupt change of several NE-SW trending boundaries.

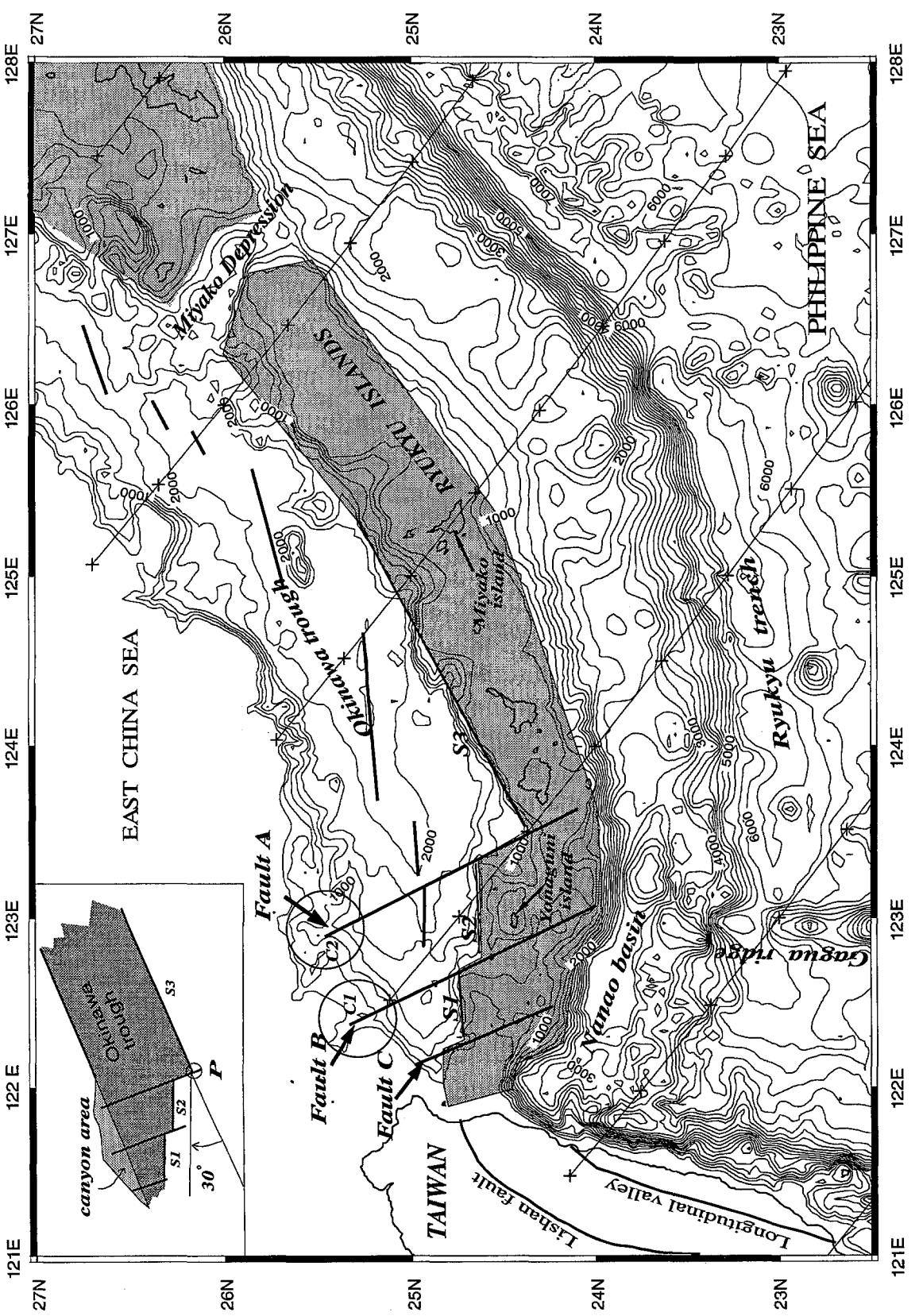

Fig. 11. Bathymetric map of the southwestern OT (from digital data). Heavy lines are central grabens in the OT. Lines with crosses are small circles of the motion of the Philippine Sea plate with respect to the Eurasian plate. Cross interval is 0.92 M.y. (after Seno *et al.*, 1993). The shaded area is the RA. C1 and C2 indicate location of canyons.

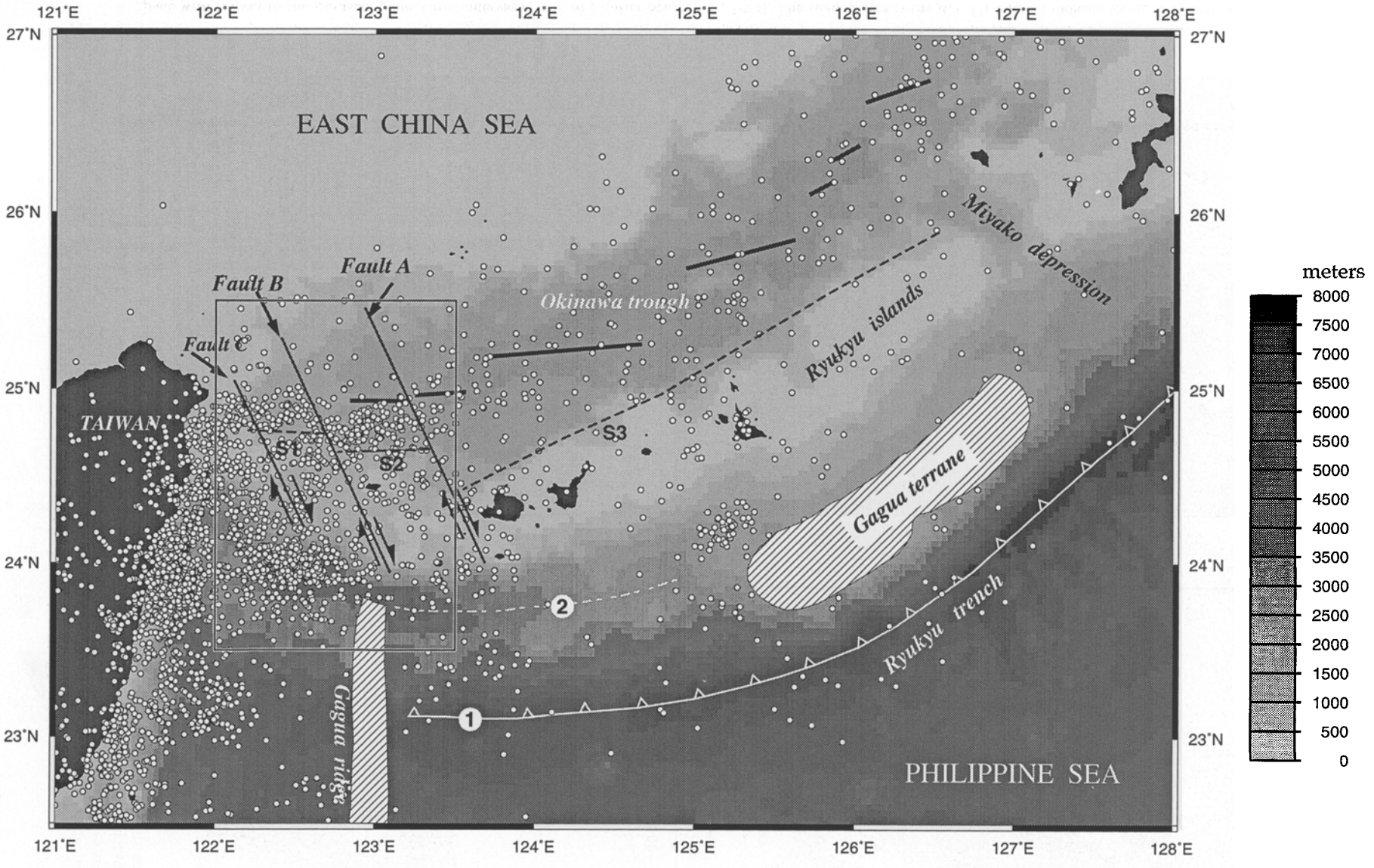

Fig. 12a. Distribution of earthquakes (small circles) of magnitude larger than 4. Dashed lines correspond to segments S1, S2 and S3 defined in Figure 11. 1: propagating trench. 2: trace of the former retreating trench.

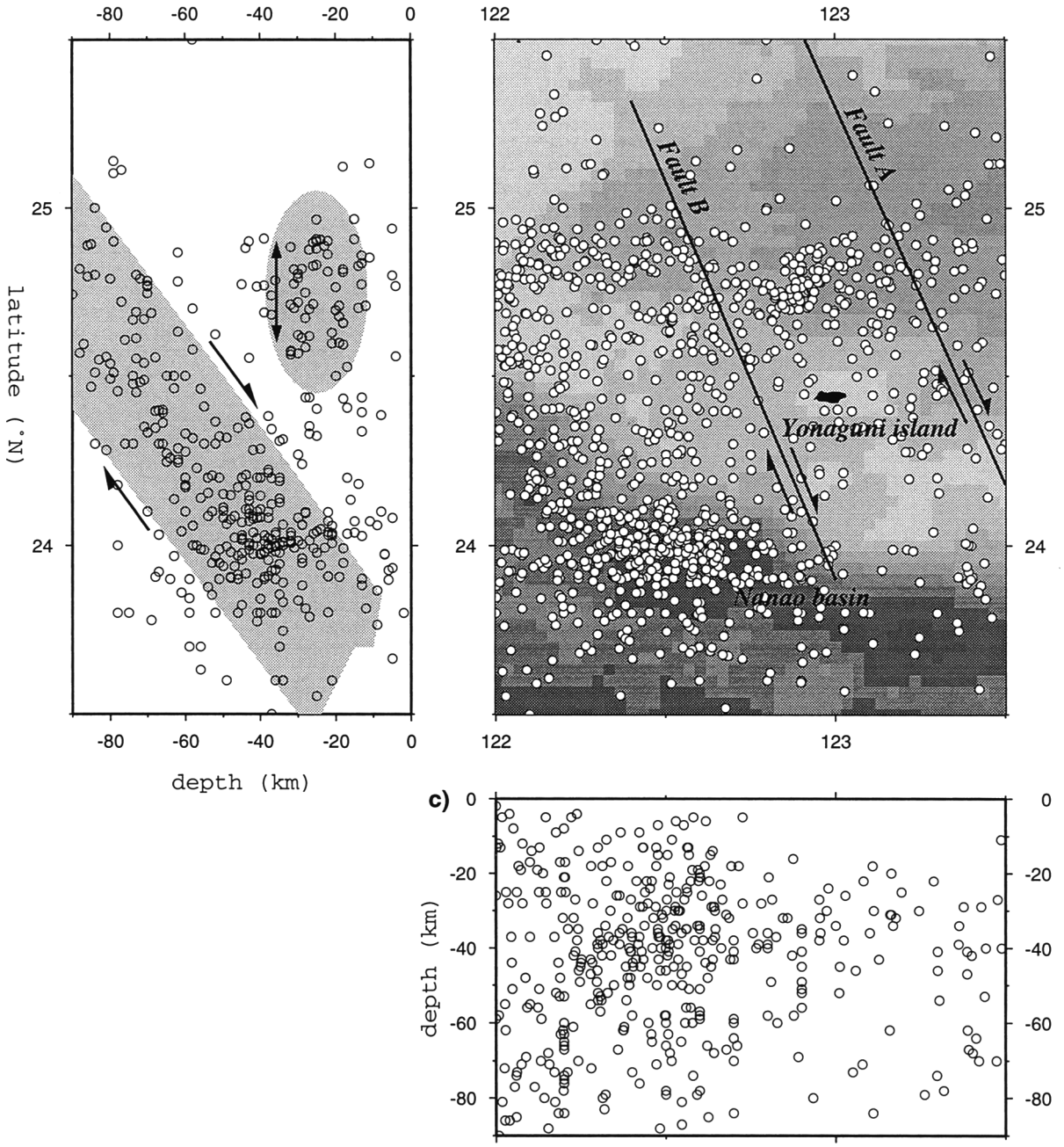

Fig. 12b. Three-dimensional distribution of the earthquakes occurring in the TRFZ. (a) Plan view distribution, superposed with shaded bathymetry. (b) Earthquake depth distribution projected perpendicular to a meridian. Elliptical shaded area represents extensional mechanism due to back-arc extension. Slab shaded area represents the Benioff zone with compressional mechanism (after Cheng *et al.*, 1992). Note that Fault A separates two groups of earthquakes in the OT and the earthquake depth in the OT is around 25 km. (c) Earthquake depth distribution projected perpendicularly to a parallel. A large number of earthquakes occurs west of the Fault B.

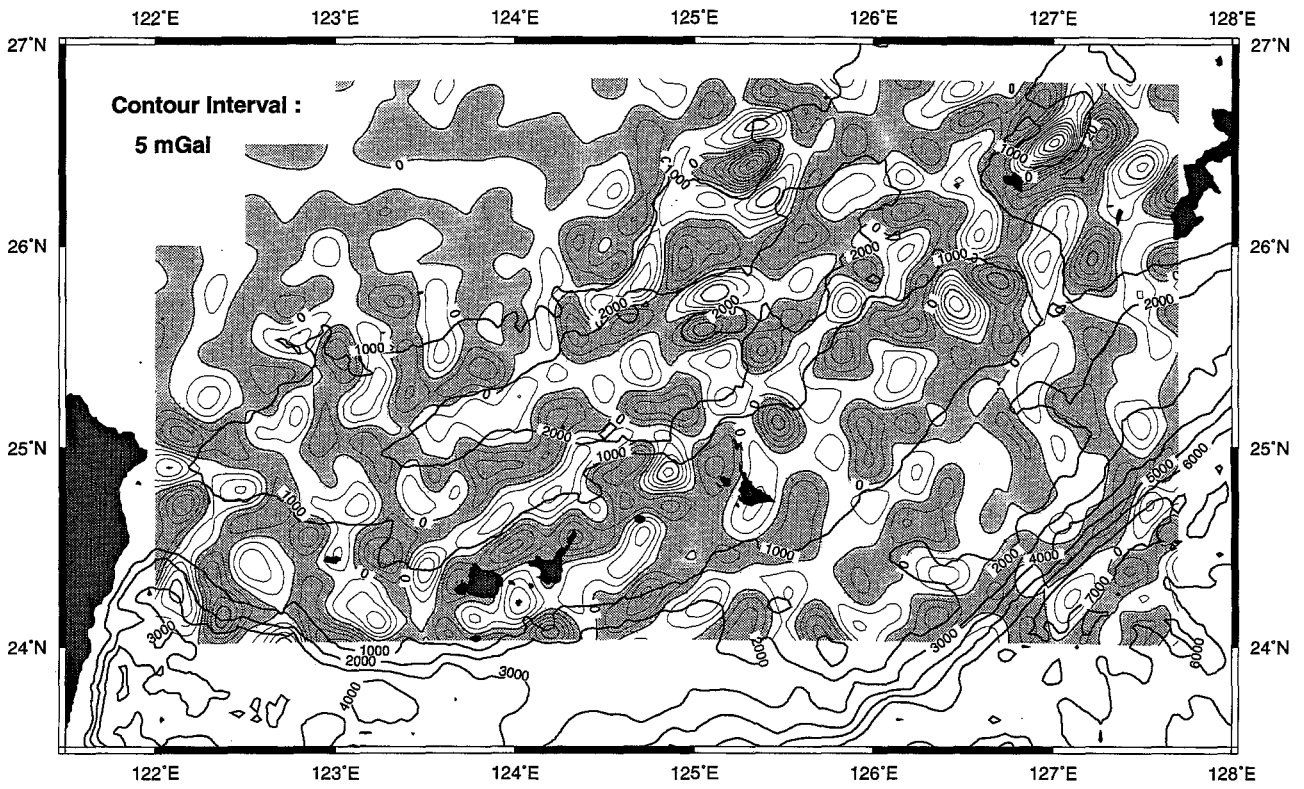

Fig. 13. Filtered Bouguer gravity anomaly of the southwestern OT. The filtered wavelength is 20–60 km. Positive values are shaded. The bathymetry is superposed. Note that, west of 123.5° E, the structural trends of the OT are roughly NW-SE oriented while, east of 123.5° E, features are trending ENE-WSW.

5.2. Bending model of the southwestern Ryukyu arc

Because the convergent rate near the bent RA (about 70 mm/yr) (Seno *et al.*, 1993) is an order larger than the average rifting rate of the OT (about 7 mm/yr) (Sibuet *et al.*, 1995), the progressive NW bending and faulting on the southwestern RA should have induced the progressive narrowing of the southwestern OT and the continental shelf region, which may explain the triangular form of the southwestern OT and Ilan plain (Figures 2b and 11). Thus, the western end of the OT in the Ilan plain would correspond to the complete closure of the OT backarc basin, due to the collision by the northern tip of the Luzon arc pushing and bending the southwestern RA in the N 310° direction (i.e. the direction of convergence of the Philippine Sea plate relative to the Eurasia plate) (Figure 15). Because Faults A, B and C display consecutive dextral strike-slip motions toward Taiwan (right-lateral stepping), it suggests that the horizontal compressional stress acting on the southwestern RA gradually increased westward. Accordingly, the downward component of the subduction with respect to the horizontal component should reach its minimum value at the intersection of the western end of the Ryukyu trench (the Nanao basin) and the northern end of the Longitudinal valley (in Taiwan). This indicates that the subduction system gradually evolved into a collisional system. However, based on the occurence of abnormal quantity of the extensional earthquakes in the southern OT (Cheng *et al.*, 1992) and in the Ilan plain (Tsai *et al.*, 1975; Yeh *et al.*, 1991), the low velocity upper mantle wedge under the Ilan plain deduced from a tomographic study (Rau and Wu, 1995) and the geodetic observations in northeastern Taiwan (Yu *et al.*, 1995), the extensional process within the southwesternmost OT has probably resumed after the Luzon arc has swept the whole south- western RA. Presently, the collision of the

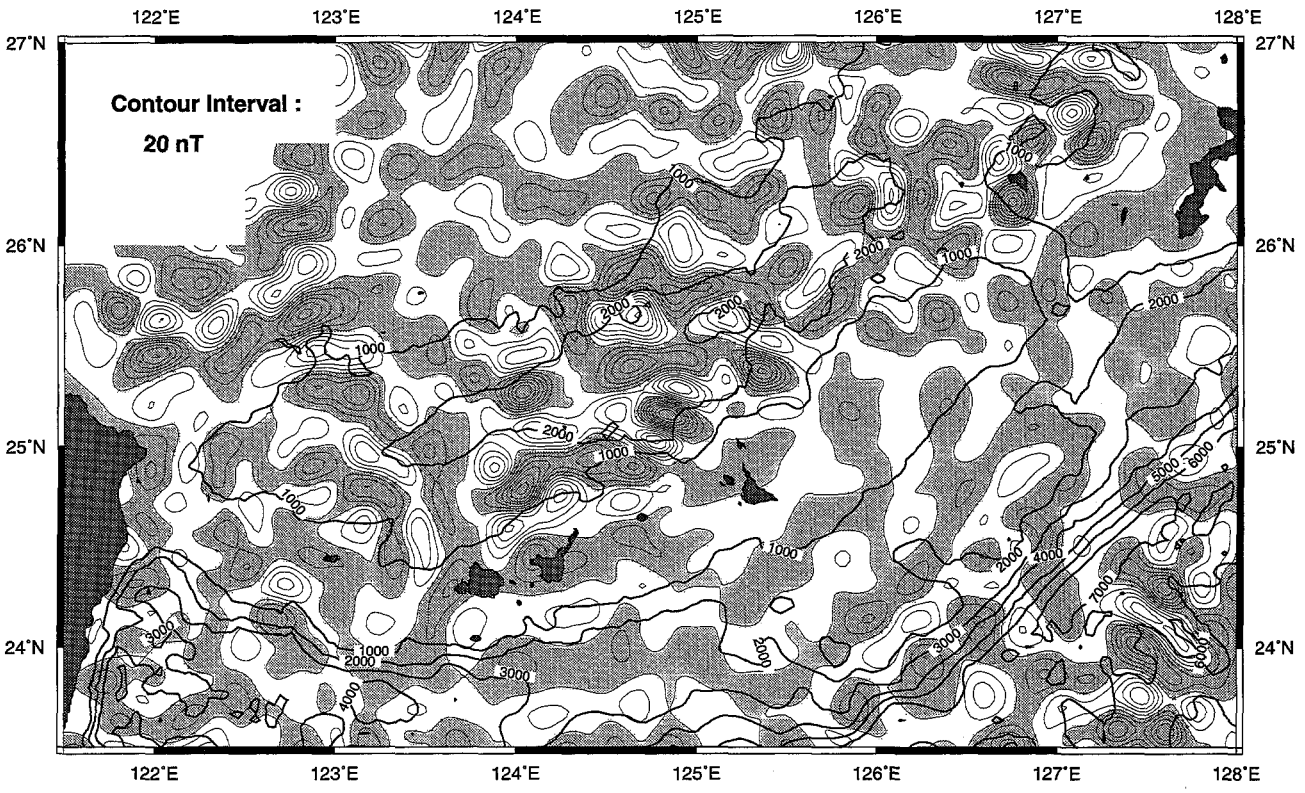

Fig. 14. Filtered magnetic anomaly of the southwestern OT. The filtered wavelength is 20–60 km. Positive values are shaded. The bathymetry is superposed. Note that, west of 123.5° E, the structural trends of the OT are roughly NW-SE oriented while, east of 123.5° E, features are trending ENE–WSW. Results are similar to those of the filtered gravity anomaly.

Luzon arc mainly concentrates in central Taiwan (at about 23° N; 12.2° E) (Yu *et al.*, 1995).

A tentative model for the collision between the Luzon arc and the ancient RA is proposed in Figures 15 and 16. The initial collision between the Luzon arc and the ancient RA could occur near 123.5° E. The large buoyancy of the Luzon arc has subsequently indented and bent the ancient RA and shortened the southern OT, generating several dextral strike-slip faults (Faults A, B and C). When Fault C occurred, the counterclockwise rotated portion of the ancient RA located west of the Luzon arc was rather parallel to the Luzon arc and most of the southwestern portion of the backarc basin was rather closed. This situation should have increased the contact surface and friction between the Luzon arc and the ancient RA (present-day Tananao complex), starting the uplift of Taiwan. Likewise, as shown by the satellite derived structural map of Taiwan (see Tsai, 1986), dextral strike-slip faults and folds resulting from the Luzon arc collision are observed in northern Taiwan. Such a mechanism, which produces brittle deformation in terms of dextral strike-slip faults, can also be observed on sandbox experiments near the free border of a rigid indenter (Lu and Malavieille, 1994).

6. Gagua Ridge and Gagua Terrane

The Gagua aseismic ridge is a pronounced NS trending feature located east of Taiwan along the 123° E meridian (Figures 1 and 2a). This linear ridge is composed of several adjacent seamounts and segments of ridges. A bathymetric difference of about 1000 m is observed between the two sides of the Gagua ridge (Figure 2a) which acts as a dam for the eastward transportation of sediments coming from eastern Taiwan. The oceanic domain located west of the Gagua ridge (Gagua basin) is under compression on the basis of earthquake focal mechanisms (Yeh *et al.*, 1991) but seismic data collected by the National Taiwan University do not display any sign of compression (S. Lallemand, personal

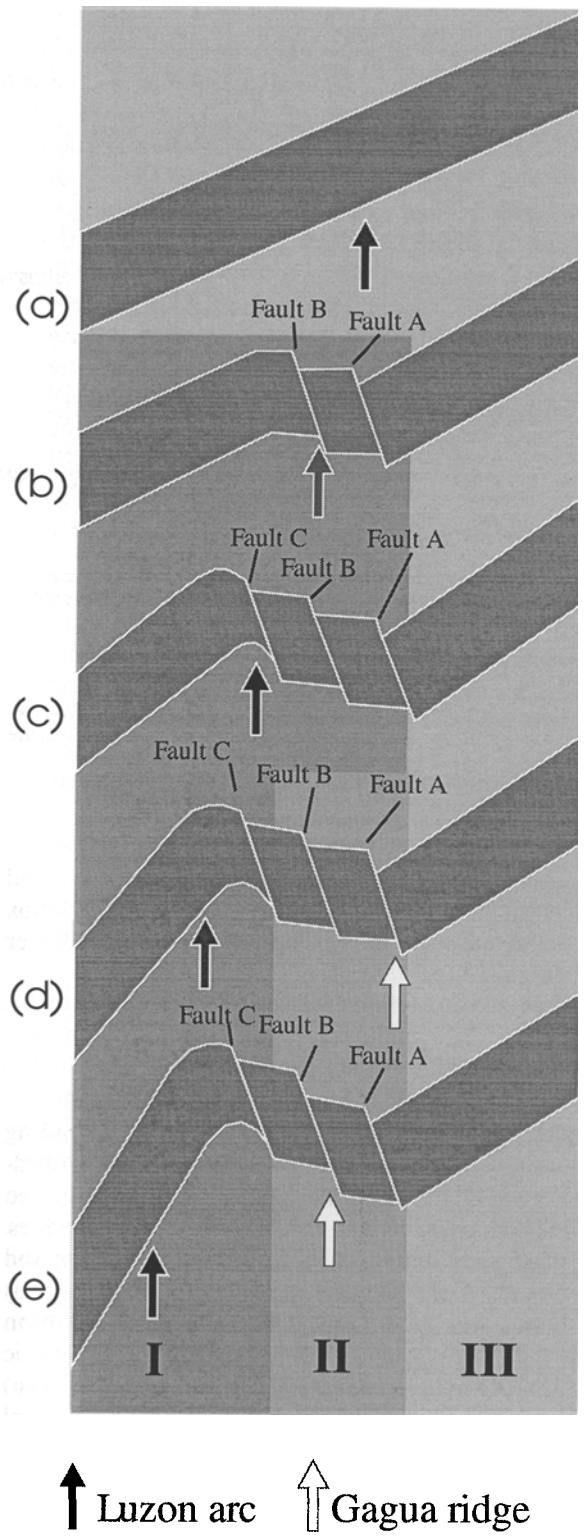

Fig. 15. Schematic tectonic deformation and evolution of the south RA. Region I is the region largely affected by the collision of the Luzon arc in Taiwan. Region II is the region of dextral strike-slip faults slightly reactivated by the collision of the Gagua ridge. Region III is undeformed. (a) Before the deformation, the RA was roughly NE-SW trending and the oceanic domain of the Philippine Sea subducted beneath the Okinawa platelet. (b) East of the Luzon arc, the RA started to bend clockwise while west of the Luzon arc the former RA started to bend counterclockwise. The clockwise deformation is accompanied by the occurrence of dextral strike-slip faults. (c) At the end of bending and faulting of the RA the western bent RA is rather parallel to the Luzon arc. This situation increased the friction between the two features and the uplift of Taiwan started at that time. (d) The collision of the Gagua ridge could have reactivated the dextral strike-slip fault A. (e) Present-day configuration of the RA. Fault B have been recently reactivated.

communication). However, this question is still debated.

Because the collision of the Gagua ridge could also change local stress conditions on the RA, Faults A and B may have been reactivated. In this hypothesis, taking into account the relative motion of the Philippine Sea plate with respect to the Eurasian plate (Seno *et al.*, 1993), Fault A may have been reactivated about 1 M.y. ago. Because each fault could release external contraint (stress) on its eastern side, the OT could rift or extend more freely on the eastern side.

The hypothesis of the Gagua terrane and along-axis propagating trench

A peculiar forearc feature, about 250-km long, located near 24.5° N; 126° E, displays a strong positive gravity anomaly and low seismicity (Figures 7a and 12). These properties are similar to those of stable oceanic plateaus present in today's oceans (e.g. Ben-Avraham *et al.*, 1983). We suggest that this stable feature, named here the Gagua terrane, could be part of the former Gagua ridge. If we trace back the Gagua ridge along small circles of the Philippine Sea plate relative to the Eurasian plate, the Gagua ridge was roughly south of the Gagua terrane about 9–4 M.y. ago. Accordingly, the former Gagua ridge would have collided with the RA during this period and resisted to subduct beneath the Okinawa platelet. In this hypothesis, the Gagua terrane, which was scraped from the Philippine Sea plate, was finally accreted against the forearc about 4 M.y. ago. In the above consideration, the former Gagua ridge was a large oceanic ridge with a small tail like the today's Oki-Daito ridge in the Philippine Sea. However, in the absence of any information about the geological nature of the Gagua terrane, a possibility still exits that this exotic terrane was part of the former Luzon arc.

During the accretion of this exotic terrane, a segment of the former Ryukyu trench became a suture zone and a new segment of the trench might appear south of it. After the emplacement of the Gagua terrane, the Gagua ridge resumed to subduct and the Ryukyu trench was segmented into two portions. When the Gagua ridge moves northwestward with respect to the Eurasian plate, the eastern segment of the Ryukyu trench propagated westward along the trench axis while the western segment retreated westward (Figures 12a and 16). On the basis of the topographic continuity between the northern end of the Longitudinal valley and the western end of the Nanao basin and the extremely low values of the gravity anomaly in the Nanao basin, the western segment should locate somewhere near the Nanao basin; however, it is noted that the orientations of both the Nanao basin and the bent RA are rather parallel to the direction of the present-day NW motion of the Philippine Sea plate relative to Eurasia (Figure 11). The present-day position of the trench is, hence, difficult to identify west of the Gagua ridge. This implies that, west of the Gagua ridge, the portion of the former convergent boundary could be considered today as a segment of transform margin, which explains why the Ryukyu trench is well recognized east of 123° E and poorly expressed west of the Gagua ridge. However, because a Benioff zone can be observed there (Figure 12b), a possibility still exists that a portion of the Luzon arc would have already subducted beneath the Ryukyu subduction zone before the collision started in Taiwan.

7. Conclusions

A new bathymetric map around Taiwan has been compiled by using available data and a careful analysis of their quality. With respect to previously published bathymetric maps, new features as seamounts and rift features belonging to the northwestern Philippine Sea domain have been identified, the morphology of the Luzon arc and associated features is better defined and a clear image of the Gagua ridge and the identification of the Gagua exotic terrane have been also evidenced on gravity and magnetic data.

The main points resulting from the interpretation of the geophysical data in the southernmost Ryukyu subduction zone are:

1. The collision of the buoyant Luzon arc with the former Ryukyu subduction zone could start near 123.5° E. The subsequent collision has resulted in the indentation and faulting of the RA and the shortening of the corresponding portion of backarc basin. Before the uplift of Taiwan, the southwestern RA bent clockwise at about 30° around a pole located near 24° N; 123.6° E and several dextral strike-slip faults probably developed during this process.
2. Based on a joint analysis of the bathymetric, magnetic, gravity and earthquake data, three major dextral strike-slip faults (Faults A, B and C) have been identified in the TRFZ. Faults A, B and C were active during the collision of the Luzon arc. Faults A and B were probably reactivated during the northward motion of the Gagua ridge.

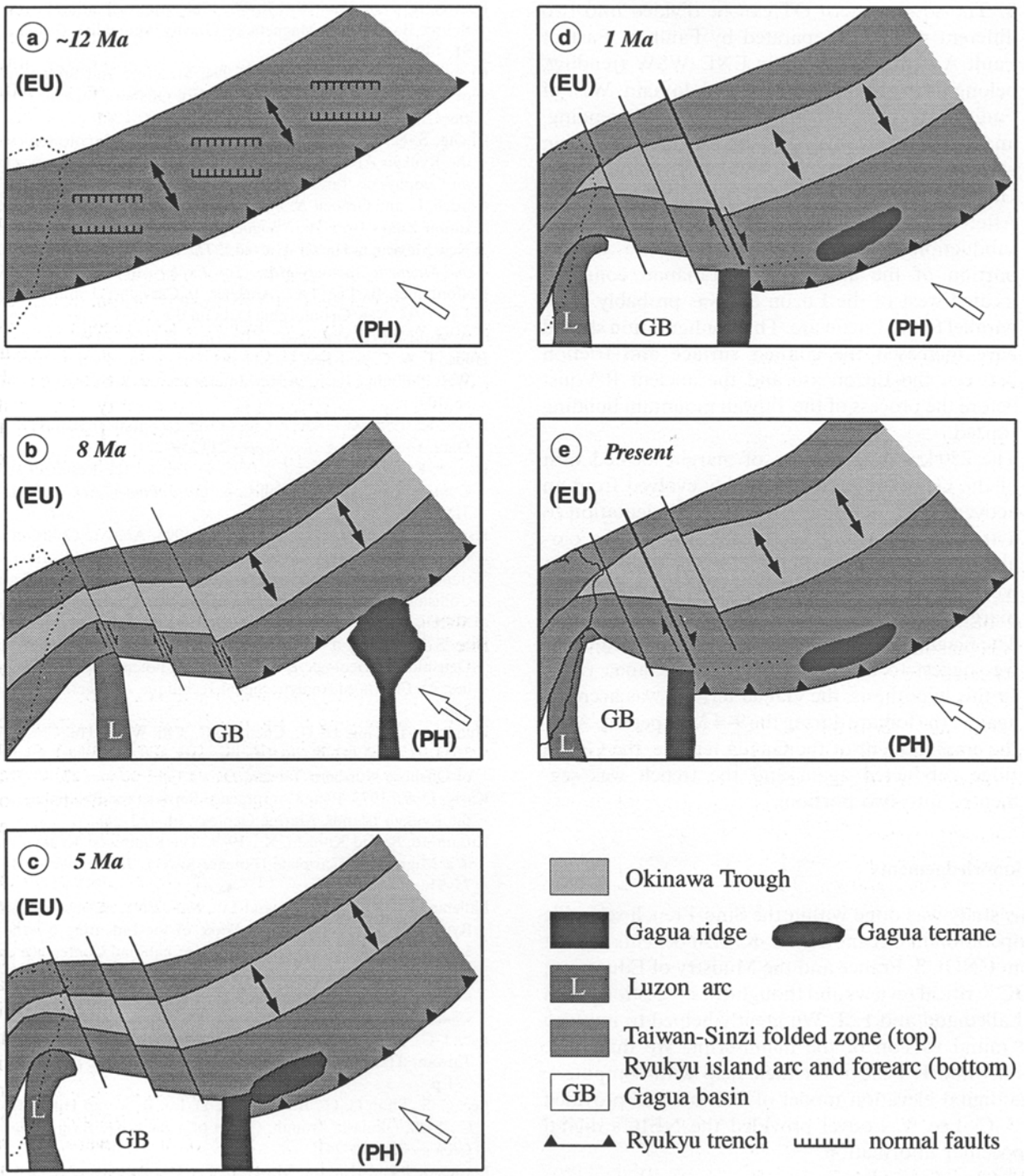

Fig. 16. Schematic evolution of the southwestern OT with the motions of the Luzon arc and Gagua ridge. (a) Initial opening of the OT. (b) Bending and faulting of the Ryukyu arc because of the collision of the Luzon arc. (c) Beginning of the Taiwan mountain building, emplacement of the Gagua terrane. (d) Propagation of the eastern segment of the Ryukyu trench along the trench axis and the retreat of the western segment. Fault A is reactivated. (e) Present-day situation. Fault B is reactivated. EU: Eurasian plate. PH: Philippine Sea plate. Open arrows indicate the motion of the PH with respect to the EU. The mean rifting direction in the OT, proposed by Sibuet *et al.* (1995), is plotted.

3. The southwestern OT can be divided into two different provinces separated by Fault A. East of Fault A, features, generally ENE–WSW trending, belong to the backarc extensional domain. West of Fault A, features are generally NW–SE trending, and are probably related to the Luzon arc collision with the Ryukyu arc and the later motion of the Gagua ridge.
4. After the indentation and faulting of the Ryukyu subduction zone, the counterclockwise rotated portion of the ancient RA (Tananao complex) located west of the Luzon arc was probably more parallel to the Luzon arc. This configuration should have increased the contact surface and friction between the Luzon arc and the ancient RA just before the process of the Taiwan mountain building started.
5. The 250 km long portion of margin located west of the Gagua ridge has probably evolved from an active margin before the Luzon arc indentation to a transform margin, as attested now by the parallelism between the Philippine Sea plate motion with respect to Eurasia and the orientation of this margin.
6. The Gagua terrane is a peculiar forearc feature that we suggest to belong to the former Gagua ridge. In this hypothesis, the Gagua terrane was accreted against the forearc during the 9–4 M.y. period. After the emplacement of the Gagua terrane, the Gagua ridge subducted again and the trench was segmented into two portions.

Acknowledgements

This study was done within the Sino-French scientific cooperation in Oceanology. S.-K. Hsu benefits a grant from CNOUS, France and the Ministry of Education, ROC. Critical reviews and thoughtful suggestions from S. Lallemand and F. T. Wu greatly helped to improve the initial version of the manuscript. We thank M. Voisset and P. Pelleau for their help with computers. The digital elevation model of Taiwan was provided by J.-C. Lee. V. Louvel provided the NEIC's digital hypocenter information.

References

Angelier, J., 1990, Geodynamic Evolution of the Eastern Eurasian Margin (Foreword), *Tectonophysics* **83**, VII-X.

Ben-Avraham, Z., Nur, A., Jones, D. and Cox, A., 1981, Continental Accretion: From Oceanic Plateaus to Allochonous Terranes, *Science* **213**, 47–54.

Blakely, R. J. and Simpson, R. W., 1986, Approximating Edges of Source Bodies from Magnetic or Gravity Anomalies, *Geophysics* **51**, 1494–1498.

Chen, T.-T. and Watkins, J. S., 1994, Structure and Stratigraphy of South Pengchiahsu Basin, Northern Offshore Taiwan, *Petrol. Geol., Taiwan* **29**, 127–170.

Cheng, S.-N., Lee, C.-T. and Yeh, Y.-T., 1992, Seismotectonics of the Ryukyu Arc. Proceeding of the Fourth Taiwan Symposium on Geophysics, Taiwan, pp. 507–516.

Cordell, L. and Grauch, V. J. S., 1985, Mapping Basement Magnetization Zones from Aeromagnetic Data in the San Juan Basin, New Mexico, in Hinze, W. J. (ed.), *The Utility of Regional Gravity and Magnetic Anomaly Maps: Soc. Explor. Geophys*, pp. 181–197.

Deffontaines, B., Lee, J.-C., Angelier, J., Carvalho, J. and Rudant, J. P., 1994, New Geomorphic Data on the Active Taiwan Orogen: A Multisource Approach, *J. Geophys. Res.* **99**, 20243–20266.

Hilde, T. W. C. and Lee, C.-S., 1984, Origin and Evolution of the West Philippine Basin: A New Interpretation, *Tectonophysics* **102**, 85–104.

Hsu S.-K., 1995, XCORR: A Cross-Over Technique to Adjust Track Data, *Computers & Geosciences* **21**, 259–271.

Hsu, S.-K. and Sibuet, J.-C., 1995, Is Taiwan the Result of Arc-Continent or Arc-Arc Collision, *Earth Planet. Sci. Lett.* **136**, 315–324.

Hsu, S.-K., Sibuet J.-C. and Monti, S., 1995, Arc-Arc Collision vs. Backarc Extension: Taiwan Mountain Building, ACT International Conference and 3rd Sino-French Symposium on Active Collision in Taiwan, Program and Extended Abstracts, 22nd-23rd March, 1995, *Geol. Soc. China, Taiwan, R. O. C.*, pp. 121–130.

Hsu, S.-K., Sibuet J.-C. and Shyu, C.-T., 1996, High-Resolution Detection of Geologic Boundaries from Potential Field Anomalies: An Enhanced Analytic Signal Technique, *Geophysics* **61**, 373–386.

Huang, S.-T., Ting, H.-H., Chen, R.-C., Chi, W.-R., Hu, C.-C. and Shen, H.-C., 1992, Basinal Framework and Tectonic Evolution of Offshore Northern Taiwan, *Petrol. Geol. Taiwan* **27**, 47–72.

Karig, D. E., 1973, Plate Convergence Between the Philippines and the Ryukyu Islands, Marine Geology **14**, 153–168.

Kuramoto, S. and Konishi, K., 1989, The Southwest Ryukyu Arc is a Migrating Microplate (Forearc Sliver), *Tectonophysics* **163**, 75–91.

Lallemand, S. E., Liu, C.-S. and Lin, S.-J., 1995, Behaviour of the Ryukyu Forearc Sliver in the Wake of the Indenting Northern Luzon Arc (East of Taiwan), ACT International Conference and 3rd Sino-French Symposium on Active Collision in Taiwan, Program and Extended Abstracts, 22nd-23rd March, 1995, *Geol. Soc. China, Taiwan, R. O. C.*, pp. 167–175.

Lee, J.-C., 1994, Structure et Déformation Active d'un Orogène: Taiwan, Thèse de Doctorat. Univ. Pierre et Marie Curie, Paris, 281 p.

Lee, C.-S., Shor, G. G., Jr., Bibee, L. D, Lu, R. S. and Hilde, T. W. C., 1980, Okinawa Trough: Origin of a Back-Arc Basin, *Marine Geology* **35**, 219–241.

Letouzey, J. and Kimura, M., 1986, The Okinawa Trough: Genesis of a Back-Arc Basin Developing Along a Continental Margin, *Tectonophysics* **125**, 209–230.

Lewis, S. D. and Hayes, D. E., 1989, Plate Convergence and Deformation, North Luzon Ridge, Philippines, *Tectonophysics* **168**, 221–237.

Lu, C.-Y. and Malavieille, J., 1994, Oblique Convergence, Indentation and Rotation Tectonics in the Taiwan Mountain Belt: Insights from Experimental Modelling, *Earth Planet. Sci. Lett.* **121**, 477–494.

Lu, R. S., Pan, J. J. and Lee C. T., 1981, Heat Flow of the Southwestern Okinawa Trough, *Earth Planet. Sci. Lett.* **55**, 299–310.

Matsumoto, T., Fujioka, K., Kimura, M., Kato, Y. and Aoki, M., 1993, Detailed Bottom Topography in the Southwesternmost Part of the Nanseishoto Trench Area, *JAMSTECR* **30**, 17–36 (in Japanese with English abstract).

Rau, R.-J. and Wu, F. T., 1995, Tomographic Images of the Lithospheric Structure Under Taiwan, *Earth Planet. Sci. Lett.* **133**, 517–532.

Sandwell, D. T., Yale, M. M. and Smith, W. H. F., 1994, ERS-1 Geodetic Mission Reveals Detailed Tectonic Structures, *EOS* **75**, Abstract, 155.

Sandwell, D. T., Yale, M. M. and Smith, W. H. F., 1995, Gravity Anomaly Profiles from ERS-1, Topex and Geosat Altimetry, *EOS* **76**, Abstract, 89.

Seno, T., Stein, S. and Gripp, A. E., 1993, A Model for the Motion of the Philippine Sea Plate with NUVEL-1 and Geological Data, *J. Geophys. Res.* **98**, 17941–17948.

Sibuet, J.-C., Letouzey, J., Barrier, F., Charvet, J., Foucher, J.-P., Hilde, T. W. C., Kimura, M., Chiao, L.-Y., Marsset, B., Muller, C. and Stephan, J.-F., 1987, Back Arc Extension in the Okinawa Trough, *J. Geophys. Res.* **92**, 14041–14063.

Sibuet, J.-C., Hsu, S.-K., Shyu, C.-T. and Liu, C.-S., 1995, Structural and Kinematic Evolutions of the Okinawa Trough Back-Arc Basin, in Taylor, B. (ed.), Backarc Basins: Tectonics and Magmatism, Plenum Press, New-York, pp. 343–379.

Smith W. H. F. and Wessel P., 1990, Gridding with Continuous Curvature Splines in Tension, *Geophysics* **55**, 293–305.

Sun, S. C., 1981, The Tertiary Basins of Off-Shore Taiwan, ASCOPE, Manila.

Suppe, J., 1984, Kinematics of Arc-Continent Collision, Flipping of Subduction, and Back-Arc Spreading Near Taiwan, *Mem. Geol. Soc. China* **6**, 21–34.

Teng, L. S., 1990, Geotectonic Evolution of Late Cenozoic Arc-Continent Collision in Taiwan, *Tectonophysics* **183**, 57–76.

Tsai, Y.-B., 1986, Seismotectonics of Taiwan, *Tectonophysics* **125**, 17–37.

Wageman, J. M., Hilde, T. W. C and Emery, K. O., 1970, Structural Framework of East China Sea and Yellow Sea, *Am. Assoc. Pet. Geol. Bull.* **54**, 1611–1643.

Wessel, P. and Smith, W. H. F., 1991, Free Software Helps Map and Display Data, *EOS* **72**, 441–446.

Wu, F. T., 1970, Focal Mechanisms and Tectonics in the Vicinity of Taiwan, *Bull. Seism. Soc. Amer.* **60**, 2045–2056.

Wu, F. T., 1978, Recent Tectonics of Taiwan, in Uyeda, S., Murphy, R. W. and Kobayashi, K. (eds.), *Geodynamics of the Western Pacific, J. Phys. Earth, Suppl. Issue,* pp. 265–299.

Yeh, Y.-H., Barrier, E., Lin, C.-H. and Angelier, J., 1991, Stress Tensor Analysis in the Taiwan Area from Focal Mechanism of Earthquakes, *Tectonophysics* **200**, 267–280.

Yen, T. P., 1975, Lithostratigraphy and Geologic Structure of Taiwan, *Geol. Paleontol. S. E. Asia* **15**, 303–323.

Yu, S.-B., Chen, H.-Y. and Kuo, L.-C., 1995, Velocity Field of GPS Stations in the Taiwan Area. ACT International Conference and 3rd Sino-French Symposium on Active Collision in Taiwan, program and Extended Abstracts, 22nd-23rd March, 1995, *Geol. Soc. China, Taiwan, R.O.C.,* pp. 317–327.